# Technical Report Series
# Center for Data and Simulation Science



**Alexander Heinlein, Axel Klawonn, Jascha Knepper, Oliver Rheinbach**


# Adaptive GDSW coarse spaces for overlapping Schwarz methods in three dimensions


Technical Report ID: CDS-2018-5
Available at `http://kups.ub.uni-koeln.de/id/eprint/8756`
Submitted on October 15, 2018

# ADAPTIVE GDSW COARSE SPACES FOR OVERLAPPING SCHWARZ METHODS IN THREE DIMENSIONS

ALEXANDER HEINLEIN[†‡], AXEL KLAWONN[†‡], JASCHA KNEPPER[†], AND OLIVER RHEINBACH[§]

**Abstract.** A robust two-level overlapping Schwarz method for scalar elliptic model problems with highly varying coefficient functions is introduced. While the convergence of standard coarse spaces may depend strongly on the contrast of the coefficient function, the condition number bound of the new method is independent of the coefficient function. Its coarse space is based on discrete harmonic extensions of vertex, edge, and face interface functions, which are computed from the solutions of corresponding local generalized edge and face eigenvalue problems. The local eigenvalue problems are of the size of the edges and faces of the decomposition, and the eigenvalue problems can be constructed solely from the local subdomain stiffness matrices and the fully assembled global stiffness matrix. The new AGDSW (Adaptive Generalized Dryja–Smith–Widlund) coarse space always contains the classical GDSW coarse space by construction of the generalized eigenvalue problems. Numerical results supporting the theory are presented for several model problems in three dimensions using structured as well as unstructured meshes and unstructured decompositions.

**Key words.** domain decomposition, multiscale, GDSW, overlapping Schwarz, adaptive coarse spaces

**AMS subject classifications.** 65F08,65F10,65N55,68W10

**1. Introduction.** We introduce an adaptive coarse space for the two-level overlapping Schwarz method [50, 53] and prove a condition number bound that is independent of heterogeneities in the coefficient function of the underlying variational problem (1); cf. section 6 and the supporting numerical results in section 9. The presented coarse space – adaptive GDSW (AGDSW) – can be regarded as an extension of the energy-minimizing GDSW coarse space (Generalized Dryja–Smith–Widlund) [7, 6], as the latter of which is always contained in the former space.

The classical GDSW coarse space is constructed by an energy-minimal extension of null space functions on the interface such that the kernel of the elliptic operator is represented. This can also be carried out algebraically and results in a method that is robust for a class of coefficient functions; cf., e.g., [6, Table 5.3] and [21, Chapter 5].

The GDSW method has been applied to a variety of model problems, see, e.g., [8, 9] for the application to linear elasticity. In [26], the use of GDSW was applied to the highly nonlinear structural part in fluid-structure interaction simulations, and in [22], it was applied to various saddle point problems. A parallel implementation of GDSW is publicly available as the FROSch [25] preconditioner (Fast and Robust Overlapping Schwarz) as part of the Trilinos [31] package ShyLU [48]; for implementation details and numerical results, see [26, 28, 27]. Furthermore, recently, in [29], a three-level parallel implementation of GDSW in two dimensions was presented. Reduced dimension GDSW coarse spaces have been considered, e.g., in [9, 5]; see also [11] and the references therein, and [30] for results on the parallel performance.

However, classical GDSW coarse spaces are not sufficient to obtain a method which is robust for arbitrary coefficient jumps; see, e.g., [21, Chapter 5]. To this end, adaptive (w.r.t. the coefficient function) coarse spaces have been developed in

[†]Department of Mathematics and Computer Science, University of Cologne, Weyertal 86-90, 50931 Köln, Germany, {alexander.heinlein, axel.klawonn, jascha.knepper}@uni-koeln.de, url: http://www.numerik.uni-koeln.de

[‡]Center for Data and Simulation Science, University of Cologne, http://www.cds.uni-koeln.de

[§]Institut für Numerische Mathematik und Optimierung, Fakultät für Mathematik und Informatik, Technische Universität Freiberg, Akademiestr. 6, 09599 Freiberg, oliver.rheinbach@math.tu-freiberg.de, http://www.mathe.tu-freiberg.de/nmo/mitarbeiter/oliver-rheinbach

the field of domain decomposition methods.

A natural initial choice for basis functions to treat coefficient variations are multiscale finite element (MsFEM) functions [33, 15]; see [1, 4, 19, 24, 16]. To define MsFEM functions, boundary values need to be chosen carefully which in [19, 24, 16] requires solving a problem on the interface. By contrast, the construction of GDSW vertex-based functions, which are included in the AGDSW space, is much simpler.

In addition to vertex-based functions, the construction of the AGDSW coarse space uses the energy-minimal extensions of low-frequency eigenmodes on the edges and faces of the domain decomposition. Note that our approach is different from the two-dimensional AGDSW coarse space in [23] which allows for a simpler implementation and can lead to smaller coarse spaces according to our numerical experiments. A special emphasis is placed on the reduction of the coarse space dimension by also integrating energy-minimal extensions into the eigenvalue problems; cf. the numerical results in section 9. This strategy has also been used for the coarse space in [24], which was inspired by a special finite element method based on approximate component mode synthesis [32].

Local generalized eigenvalue problems to construct coarse spaces have been used earlier to obtain methods which are robust to coefficient jumps. In [16], the authors present two approaches to construct coarse spaces which lead to eigenvalue problems of the same size as here. The setup of their eigenvalue problems is cheaper, however, the coarse space dimension can be significantly larger; cf. section 9. In [17], Galvis and Efendiev use generalized eigenvalue problems on unions of subdomains resulting in large eigenvalue problems. Dolean et al. proposed generalized eigenvalue problems on subdomain boundaries but a restriction on the class of coefficient functions was required to prove the condition number bound in [12]. In [51], Spillane et al. then introduced the coarse space GenEO in which they reduced the generalized eigenvalue problems to the overlap of subdomains allowing arbitrary coefficient functions. A further reduction to edges in two dimensions, and edges and faces in three dimensions, was realized in [18, 19, 24, 23, 16]. Other notable contributions to multiscale domain decomposition for overlapping Schwarz are, e.g., [20, 3]. Adaptive coarse spaces for nonoverlapping domain decomposition methods have gained much interest as well; see, e.g., [2, 43, 44, 52, 46, 36, 38, 47, 35, 37, 45].

**2. Model problem.** On a polyhedral domain $\Omega \subset \mathbb{R}^3$, we consider the variational problem: find $u \in H_0^1(\Omega)$, such that

$$a_\Omega(u,v) = L(v) \qquad \forall v \in H_0^1(\Omega), \tag{1}$$

$$\text{where} \quad a_\Omega(u,v) := \int_\Omega A(x)(\nabla u(x))^T \nabla v(x)\, dx \quad \text{and} \quad L(v) := \int_\Omega f(x) v(x)\, dx,$$

respectively, and where $A\colon \mathbb{R}^3 \to \mathbb{R}$ is a scalar coefficient function and $f \in L^2(\Omega)$. In this paper, $A$ is typically highly heterogeneous, possibly having discrete values with large variations. In addition to that, we denote the semi-norm corresponding to the bilinear form $a_\Omega(\cdot,\cdot)$ as

$$|u|_{a,\Omega}^2 := a_\Omega(u,u).$$

We assume that the coefficient function $A(x)$ satisfies

$$0 < A_{\min} \le A(x) \le A_{\max} \quad \forall x \in \overline{\Omega}.$$

Then, the Lax-Milgram lemma guarantees a unique solution of (1). Let

$$Ku = f \tag{2}$$

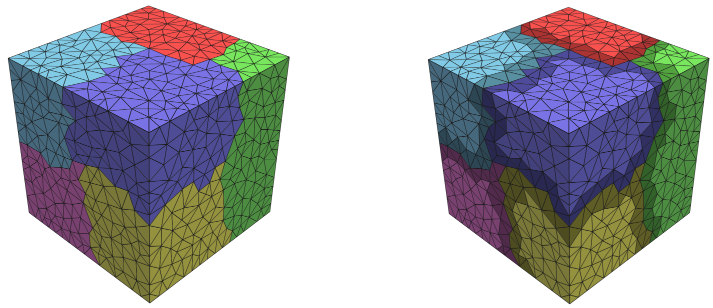

FIG. 1. *Example of a nonoverlapping domain decomposition* $\{\Omega_i\}_{i=1}^N$ ***(left)*** *and the corresponding overlapping domain decomposition* $\{\Omega_i'\}_{i=1}^N$ ***(right)*** *with overlap* $\delta = 1h$.

be the discretization of problem (1) by piecewise linear or trilinear finite elements on a triangulation $\tau_h$. Here, $K$ is the stiffness matrix, $f$ the right hand side, and $u$ the vector corresponding to the finite element solution in the finite element space $V^h(\Omega)$. Throughout this paper, we assume that the coefficient function $A$ is constant on each finite element $T \in \tau_h$. However, our method is not restricted to these cases. In order to solve this problem, we use the conjugate gradient method preconditioned by a two-level overlapping Schwarz preconditioner.

**3. Two-level overlapping Schwarz methods.** Let $\{\Omega_i\}_{i=1}^N$ be a nonoverlapping domain decomposition of $\Omega$ into polyhedral subdomains $\Omega_i$ with a typical subdomain diameter of $H$. The interface $\Gamma$ of the nonoverlapping domain decomposition is defined as $\Gamma = \bigcup_{i=1}^N \partial\Omega_i \setminus \partial\Omega$.

Next, we obtain a corresponding overlapping decomposition $\{\Omega_i'\}_{i=1}^N$ of $\Omega$ by extending the nonoverlapping subdomains by $k$ layers of finite elements. This results in an overlap $\delta = kh$; cf. Figure 1. We define as $R_i : V^h(\Omega) \to V_i := V^h(\Omega_i')$, $i = 1, ..., N$, the restriction to the local finite element space on the overlapping subdomain $\Omega_i'$; $R_i^T$ is the corresponding prolongation to $V^h(\Omega)$. In addition, let $V_0$ be some global coarse space and $R_0 : V^h(\Omega) \to V_0 \subset V^h(\Omega)$ the corresponding coarse interpolation. We use exact solvers, and therefore the local and coarse bilinear forms on the subspaces are given by

$$\tilde{a}_i(u_i, v_i) = a_\Omega\left(R_i^T u_i, R_i^T v_i\right) \quad \forall u_i, v_i \in V_i,$$

$i = 0, ..., N$. Then, the additive two-level Schwarz operator is given by

$$P_{\mathrm{OS-2}} = M_{\mathrm{OS-2}}^{-1} K = R_0^T K_0^{-1} R_0 + \sum_{i=1}^N R_i^T K_i^{-1} R_i K$$

with local stiffness matrices $K_i = R_i K R_i^T$, for $i = 1, ..., N$; cf. [53, Chapter 2.2] and coarse operator $K_0 = R_0 K R_0^T$.

The condition number of the two-level Schwarz operator for the finite element problem (2) using Lagrangian coarse basis functions for $K_0$ depends on the contrast of the coefficient function $A$, i.e.,

$$\kappa\left(M_{\mathrm{OS-2}}^{-1} K\right) \le C \max_{T \in \tau_H} \max_{x,y \in \omega_T} \left(\frac{A(x)}{A(y)}\right)\left(1 + \frac{H}{\delta}\right);$$

cf. [20]. Here, $\tau_H$ corresponds to the set of all coarse mesh elements, and $\omega_T$ to the union of all coarse mesh elements which touch a coarse mesh element $T$. This bound can be improved but a dependence on the coefficient contrast remains.

**4. The GDSW preconditioner.** The GDSW preconditioner [6, 7] is a two-level additive overlapping Schwarz preconditioner with exact solvers as described in the previous section. Thus, the preconditioner can be written in the form

$$M_{\text{GDSW}}^{-1} = \Phi K_0^{-1} \Phi^T + \sum_{i=1}^{N} R_i^T K_i^{-1} R_i,$$

where $\Phi = R_0^T$. Here, the columns of $\Phi$ are coefficient vectors corresponding to the coarse basis functions and the main ingredient of the GDSW preconditioner.

The interface can be decomposed as $\Gamma = \left(\bigcup_{f \in \mathcal{F}} f\right) \cup \left(\bigcup_{e \in \mathcal{E}} e\right) \cup \left(\bigcup_{v \in \mathcal{V}} v\right)$, where $\mathcal{F}$ is the set of all faces, $\mathcal{E}$ the set of all edges, and $\mathcal{V}$ the set of all vertices; see, e.g., [41, Sect. 3] and [39, 40, Sect. 2]. The discrete characteristic functions $\chi_*^h$ of the vertices, edges, and faces form a partition of unity on $\Gamma$, i.e.,

$$1 = \sum_{v \in \mathcal{V}} \chi_v^h + \sum_{e \in \mathcal{E}} \chi_e^h + \sum_{f \in \mathcal{F}} \chi_f^h.$$

Let the columns of the matrix $\Phi_\Gamma$ be the coefficient vectors of the partition of unity functions; then, the matrix $\Phi_\Gamma$ has only entries 0 and 1. We extend the interface values to the interior using discrete harmonic extensions. The discrete harmonic extension $w := \mathcal{H}_{\Gamma \to \Omega}(\tau_\Gamma)$ of a finite element function $\tau_\Gamma$ on the interface with respect to the bilinear form $a_\Omega(\cdot, \cdot)$ is given by

$$\begin{aligned} a_{\Omega_l}(w, v) &= 0 \qquad \forall v \in V_0^h(\Omega_l), l = 1, ..., N, \\ w &= \tau_\Gamma \quad \text{on } \Gamma. \end{aligned} \tag{3}$$

Note that a discrete harmonic extension is energy-minimal, i.e., it is

$$a_\Omega(\mathcal{H}_{\Gamma \to \Omega}(\tau_\Gamma), \mathcal{H}_{\Gamma \to \Omega}(\tau_\Gamma)) \leq a_\Omega(v, v) \quad \forall v \in \{v \in V^h(\Omega) : v|_\Gamma = \tau_\Gamma\};$$

see, e.g., [53, Sect. 4.4]. In matrix form, the discrete harmonic extension of $\Phi_\Gamma$ can be computed as

$$\Phi = \begin{bmatrix} \Phi_I \\ \Phi_\Gamma \end{bmatrix} = \begin{bmatrix} -K_{II}^{-1} K_{\Gamma I}^T \Phi_\Gamma \\ \Phi_\Gamma \end{bmatrix}.$$

Typically, $K_{II}^{-1} K_{\Gamma I}^T$ is not built explicitly but evaluated from right to left in the application of $K_{II}^{-1} K_{\Gamma I}^T \Phi_\Gamma$. The matrix $K_{II} = \text{diag}_{i=1}^N (K_{II}^{(i)})$ is a block diagonal and contains only the local matrices $K_{II}^{(i)}$ from the nonoverlapping subdomains. Therefore, the factorization of $K_{II}$ can be computed block-by-block and in parallel.

The condition number estimate for the GDSW preconditioner

$$\kappa\left(M_{\text{GDSW}}^{-1} K\right) \leq C \left(1 + \frac{H}{\delta}\right) \left(1 + \log\left(\frac{H}{h}\right)\right)^2,$$

cf. [6, 7], holds also for the general case of $\Omega$ decomposed into John domains (in two dimensions), and thus, in particular, for unstructured domain decompositions. Note that, in general, the constant $C$ depends on the contrast of the coefficient function $A$. As a remedy, we will employ the eigenmodes of local generalized eigenvalue problems to compute an adaptive coarse space that is robust, independent of the coefficient function.

**5. Adaptive GDSW.** In this section, we will introduce the adaptive GDSW (AGDSW) coarse space. Note that we have improved the AGDSW coarse space compared to the variant introduced in [23] for two dimensions. In particular, the

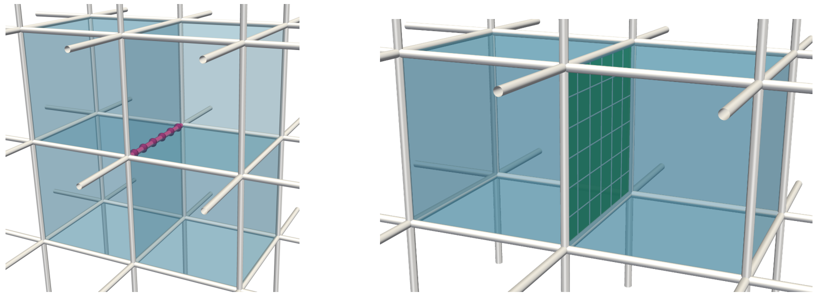

FIG. 2. *Graphical representation of $\Omega_e = \bigcup_{k\in n^e} \Omega_k$, the union of all subdomains adjacent to an open edge (**left**), and $\Omega_f = \Omega_i \cup \Omega_j$, the union of all subdomains adjacent to an open face (**right**).*

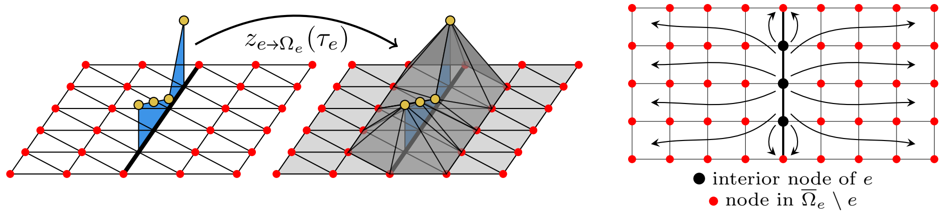


FIG. 3. *Graphical representation in two dimensions of the extension by zero of a finite element function defined on an edge $e \in \mathcal{E}$, from the interior degrees of freedom of the edge to the adjacent subdomains (**left**). Graphical representation in two dimensions of the discrete harmonic extension (4) from the interior degrees of freedom of an edge $e \in \mathcal{E}$ to $\Omega_e$ (**right**).*

construction of the eigenvalue problems was simplified. For more details, see section 7. We remark that the proofs for the condition number estimate for the two-dimensional case and for the variant introduced in [23] are analogous to the proof presented here for the 3D case.

**5.1. Construction of the AGDSW coarse space.** First, we will introduce a generic local generalized eigenvalue problem which is set up for any interface component, i.e., for any edge or face. The coarse basis functions are then constructed as discrete harmonic extensions of corresponding eigenmodes.

Let $\xi$ be an (open) edge $e$ or (open) face $f$. We denote the set of indices of adjacent subdomains by $n^e$, $n^f$, and $n^\xi$, respectively. Then, we define the set $\Omega_\xi$ as the union of all adjacent subdomains; cf. Figure 2. Additionally, we define the following extension-by-zero operator from $\xi$ to a connected set $G \subset \Omega$ with $\xi \subset G$:

$$z_{\xi\to G} : V^h(\xi) \to V_0^h(G),\ v \mapsto z_{\xi\to G}(v) := \begin{cases} v & \text{in all interior nodes of } \xi, \\ 0 & \text{on all other nodes in } G; \end{cases}$$

see Figure 3 (left) for a graphical representation in 2D. Here,

$$V_0^h(G) := \left\{ v|_G : v \in V^h(\Omega), v = 0 \text{ in } \Omega \setminus G \right\}.$$

By $\mathcal{H}_{\xi\to\Omega_\xi}$ we denote the discrete harmonic extension w.r.t. $a_\Omega(\cdot,\cdot)$ from $\xi$ to $\Omega_\xi$. Specifically, let $V_{0,\xi}^h(\Omega_l) := \{w|_{\Omega_l} : w \in V^h(\Omega), w = 0 \text{ on } \xi\}$. Then, for $\tau_\xi \in V^h(\xi)$ the extension $v_\xi := \mathcal{H}_{\xi\to\Omega_\xi}(\tau_\xi)$ is given by the solution of

$$\begin{aligned} a_{\Omega_l}(v_\xi, v) &= 0 \quad \forall v \in V_{0,\xi}^h(\Omega_l), l \in n^\xi, \\ v_\xi &= \tau_\xi \quad \text{on } \xi, \end{aligned} \tag{4}$$

where $n^\xi$ is the set of indices of all subdomains adjacent to the edge or face $\xi$. Note that, in contrast to (3), we do not prescribe Dirichlet boundary values on $\Gamma \setminus \xi$.

In particular, the boundary nodes of $\xi$ are part of the Neumann boundary of the discrete harmonic extension $\mathcal{H}_{\xi\to\Omega_\xi}$; cf. Figure 3 (right). This is different from [23], where finite elements adjacent to the vertices are removed; also see [23, Fig. 1]. Our new approach allows to construct the left hand side of the eigenvalue problem from the assembled subdomain stiffness matrix.

Now, we consider the generalized eigenvalue problem on each edge or face $\xi$: find $\tau_{*,\xi} \in V_0^h(\xi) := \left\{ v|_\xi : v \in V^h(\Omega), v = 0 \text{ on } \partial\xi \right\}$ such that

$$a_{\Omega_\xi}\left(\mathcal{H}_{\xi\to\Omega_\xi}(\tau_{*,\xi}), \mathcal{H}_{\xi\to\Omega_\xi}(\theta)\right) = \lambda_{*,\xi} a_{\Omega_\xi}\left(z_{\xi\to\Omega_\xi}(\tau_{*,\xi}), z_{\xi\to\Omega_\xi}(\theta)\right) \quad \forall \theta \in V_0^h(\xi)\,. \tag{5}$$

Let the eigenvalues be sorted in non-descending order, i.e., $\lambda_{1,\xi} \leq \lambda_{2,\xi} \leq \ldots \leq \lambda_{m,\xi}$, and the eigenmodes accordingly, where $m = \dim\left(V_0^h(\xi)\right)$. Furthermore, let the eigenmodes $\tau_{*,\xi}$ satisfy $a_{\Omega_\xi}(z_{\xi\to\Omega_\xi}(\tau_{k,\xi}), z_{\xi\to\Omega_\xi}(\tau_{j,\xi})) = \delta_{kj}$, where $\delta_{kj}$ is the Kronecker delta symbol. We select all eigenmodes $\tau_{*,\xi}$ where the eigenvalues are below a certain threshold, i.e., $\lambda_{*,e} \leq tol_\mathcal{E}$ for edges and $\lambda_{*,f} \leq tol_\mathcal{F}$ for faces. Then, the coarse basis functions corresponding to $\xi$ are the extensions

$$v_{*,\xi} := \mathcal{H}_{\Gamma\to\Omega}\left(z_{\xi\to\Gamma}(\tau_{*,\xi})\right) \tag{6}$$

of the selected $\tau_{*,\xi}$.

We define the space of edge based coarse functions as

$$V_\mathcal{E}^{tol_\mathcal{E}} := \left(\bigoplus_{e\in\mathcal{E}} \operatorname{span}\left\{v_{k,e} : \lambda_{k,e} \leq tol_\mathcal{E}\right\}\right). \tag{7}$$

and the space of face based coarse functions as

$$V_\mathcal{F}^{tol_\mathcal{F}} := \left(\bigoplus_{f\in\mathcal{F}} \operatorname{span}\left\{v_{k,f} : \lambda_{k,f} \leq tol_\mathcal{F}\right\}\right). \tag{8}$$

In addition to the edge and face basis functions, we use the vertex basis functions

$$\phi_v = \begin{bmatrix} -K_{II}^{-1} K_{\Gamma I}^T \chi_v^h|_\Gamma \\ \chi_v^h|_\Gamma \end{bmatrix}$$

from the GDSW coarse space, and denote the corresponding space by

$$V_\mathcal{V} := \bigoplus_{v\in\mathcal{V}} \operatorname{span}\left\{\phi_v\right\}; \tag{9}$$

see also section 4. Finally, we obtain the adaptive GDSW coarse space

$$V_{\text{AGDSW}}^{tol_\mathcal{E}, tol_\mathcal{F}} = V_\mathcal{V} \oplus V_\mathcal{E}^{tol_\mathcal{E}} \oplus V_\mathcal{F}^{tol_\mathcal{F}}.$$

Note that the left hand side of the eigenvalue problem (5) is singular, and its kernel contains the constant functions. Thus, the coarse basis functions corresponding to the eigenvalue 0 are, in fact, the classical coarse GDSW edge and face basis functions. Since $tol_\mathcal{E}, tol_\mathcal{F} \geq 0$, these are always included in the adaptive GDSW coarse space.

Remark 1. *For $tol_\mathcal{E} \geq 0$, $tol_\mathcal{F} \geq 0$, we obtain*

$$V_{\text{GDSW}} = V_{\text{AGDSW}}^{0,0} \subset V_{\text{AGDSW}}^{tol_\mathcal{E}, tol_\mathcal{F}}.$$

Remark 2. *If a Dirichlet boundary condition on $\partial\Omega$ is prescribed only on a subset $\partial\Omega_D \subset \partial\Omega$, in combination with a Neumann boundary condition on $\partial\Omega_N = \partial\Omega \setminus \partial\Omega_D$, the construction of the adaptive GDSW coarse space and the proof of the condition number estimate in section 6 are essentially the same. Finite element nodes that lie on the Neumann boundary are simply treated as interior nodes.*

**5.2. Properties of the spectral projection.** For the coarse interpolation defined in section 6, we consider the projections

$$\Pi_{\mathcal{E}} w := \sum_{e\in\mathcal{E}} \Pi_e w, \qquad \Pi_e w := \sum_{\lambda_{k,e}\leq tol_{\mathcal{E}}} a_{\Omega_e}\left(z_{e\to\Omega_e}(w), z_{e\to\Omega_e}(v_{k,e})\right) v_{k,e}, \tag{10}$$

$$\Pi_{\mathcal{F}} w := \sum_{f\in\mathcal{F}} \Pi_f w, \qquad \Pi_f w := \sum_{\lambda_{k,f}\leq tol_{\mathcal{F}}} a_{\Omega_f}\left(z_{f\to\Omega_f}(w), z_{f\to\Omega_f}(v_{k,f})\right) v_{k,f} \tag{11}$$

onto the spaces $V_{\mathcal{E}}^{tol_{\mathcal{E}}}$ and $V_{\mathcal{F}}^{tol_{\mathcal{F}}}$, respectively. Here, $v_{k,e}$ and $v_{k,f}$ are from (6).

These projections have typical properties, summarized in the following lemma. The lemma may be applied to the projections in (10) and (11); cf. Lemma 2 and Remark 3. The proof uses standard arguments from spectral theory.

Lemma 1. *Let a symmetric, positive semi-definite bilinear form $d(\cdot,\cdot)$ and a symmetric positive definite bilinear form $c(\cdot,\cdot)$ be given on a finite element space $W$ and consider the eigenvalue problem: find $v \in W$ such that*

$$d(v,w) = \lambda c(v,w) \quad \forall w \in W. \tag{12}$$

*Let the corresponding eigenpairs $\{(v_k,\lambda_k)\}_{k=1}^{\dim(W)}$ be chosen such that $c(v_k,v_j) = \delta_{kj}$, where $\delta_{kj}$ is the Kronecker delta symbol. Additionally, we assume that the eigenpairs are sorted in non-descending order w.r.t. the eigenvalues. Given $u \in W$, the operator $\Pi u := \sum_{\lambda_k\leq tol} c(u,v_k)\, v_k$ defines a projection which is orthogonal with respect to the bilinear form $d(\cdot,\cdot)$ and therefore $|u|_d^2 = |\Pi u|_d^2 + |u-\Pi u|_d^2$. Here, the semi-norm $|u|_d^2$ is defined as $|u|_d^2 := d(u,u)$. In addition, for $||u||_c^2 := c(u,u)$, the estimate holds*

$$\|u-\Pi u\|_c^2 \leq \frac{1}{tol}\, |u-\Pi u|_d^2\,.$$

Lemma 2. *Let $\xi \subset \Gamma$ be an open, connected interface component (e.g. an edge or a face) with adjacent subdomains $\Omega_i, i \in n^\xi$. Given a symmetric positive definite bilinear form $c\colon V^h(\xi)\times V^h(\xi) \to \mathbb{R}$, assume there exists a constant $C_{\mathrm{inv},\xi}$,*

$$s.t. \quad \left|z_{\xi\to\Omega_\xi}(v)\right|_{a,\Omega_\xi}^2 \leq C_{\mathrm{inv},\xi}||v||_c^2 \quad \forall\, v \in V^h(\xi). \tag{13}$$

*Furthermore, let $d\colon V^h(\xi)\times V^h(\xi) \to \mathbb{R}$ be a symmetric positiv semi-definite bilinear form which satisfies*

$$\left|z_{\xi\to\Omega_\xi}(v)\right|_d^2 \leq |v|_{a,\Omega_\xi}^2 \quad \forall\, v \in V^h(\Omega). \tag{14}$$

*Based on the eigenvalue problem (12) in Lemma 1 with $W := V_0^h(\xi)$, we have for $i \in n^\xi$ and $u \in V^h(\Omega)$*

$$\left|z_{\xi\to\Omega_\xi}(u) - \Pi z_{\xi\to\Omega_\xi}(u)\right|_{a,\Omega_i}^2 \leq \left|z_{\xi\to\Omega_\xi}(u) - \Pi z_{\xi\to\Omega_\xi}(u)\right|_{a,\Omega_\xi}^2 \leq \frac{C_{\mathrm{inv},\xi}}{tol_\xi} \sum_{k\in n^\xi} |u|_{a,\Omega_k}^2\,.$$

*Proof of Lemma 2.* Using the assumptions and Lemma 1 (third and fourth inequality), we have

$$\begin{aligned}
&\left|z_{\xi\to\Omega_\xi}(u) - \Pi z_{\xi\to\Omega_\xi}(u)\right|_{a,\Omega_i}^2 \leq \left|z_{\xi\to\Omega_\xi}(u) - \Pi z_{\xi\to\Omega_\xi}(u)\right|_{a,\Omega_\xi}^2 \\
= \;& \left|z_{\xi\to\Omega_\xi}(z_{\xi\to\Omega_\xi}(u) - \Pi z_{\xi\to\Omega_\xi}(u))\right|_{a,\Omega_\xi}^2 \overset{(13)}{\leq} C_{\mathrm{inv},\xi} \left\|z_{\xi\to\Omega_\xi}(u) - \Pi z_{\xi\to\Omega_\xi}(u)\right\|_c^2 \\
\overset{\text{Lemma 1}}{\leq} \;& \frac{C_{\mathrm{inv},\xi}}{tol} \left|z_{\xi\to\Omega_\xi}(u) - \Pi z_{\xi\to\Omega_\xi}(u)\right|_d^2 \leq \frac{C_{\mathrm{inv},\xi}}{tol} \left|z_{\xi\to\Omega_\xi}(u)\right|_d^2 \\
\overset{(14)}{\leq} \;& \frac{C_{\mathrm{inv},\xi}}{tol} |u|_{a,\Omega_\xi}^2 = \frac{C_{\mathrm{inv},\xi}}{tol} \sum_{k\in n^\xi} |u|_{a,\Omega_k}^2\,.
\end{aligned}$$

□

Remark 3. *For an edge $\xi = e$ or a face $\xi = f$, the bilinear forms are*

$$c(\cdot,\cdot) = a_{\Omega_\xi}(z_{\xi\to\Omega_\xi}(\cdot), z_{\xi\to\Omega_\xi}(\cdot)) \quad \text{and} \quad d(\cdot,\cdot) = a_{\Omega_\xi}(\mathcal{H}_{\xi\to\Omega_\xi}(\cdot), \mathcal{H}_{\xi\to\Omega_\xi}(\cdot));$$

*cf. eigenvalue problem (5). Hence, $C_{\mathrm{inv,e}} = C_{\mathrm{inv,f}} = 1$ and, due to the energy-minimal property of the discrete harmonic extension,*

$$\begin{aligned} d(z_{\xi\to\Omega_\xi}(v), z_{\xi\to\Omega_\xi}(v)) &= \left|\mathcal{H}_{\xi\to\Omega_\xi}(z_{\xi\to\Omega_\xi}(v))\right|^2_{a,\Omega_\xi} = \left|\mathcal{H}_{\xi\to\Omega_\xi}(v)\right|^2_{a,\Omega_\xi} \\ &\le |v|^2_{a,\Omega_\xi} \quad \forall v \in V^h(\Omega). \end{aligned}$$

*Thus, for the adaptive GDSW coarse space, the assumptions of Lemma 2 hold.*

*In subsection 7.1, we describe a variant of adaptive GDSW for which $C_{\mathrm{inv,e}} = C_{\mathrm{inv,f}}$ corresponds to the constant from an inverse inequality bounding $|\cdot|_{H^1(T)}$ by $||\cdot||_{L^2(T)}$ on a finite element $T$. Subsequently, in subsection 7.2, we describe a variant with a modified left hand side of the generalized eigenvalue problem. Both variants are covered by Lemma 2 and the proof of the existence of a stable decomposition in Theorem 6.*

**6. Convergence analysis for the overlapping Schwarz method with the adaptive GDSW space.** In this section, we will provide a condition number estimate and a proof of this estimate. Following, e.g., [53], we prove the existence of a stable decomposition. Therefore, we have to provide a suitable coarse interpolation $I_0$ into the coarse space

$$V_0 := V_{\mathrm{AGDSW}}^{tol_\mathcal{E}, tol_\mathcal{F}} = V_\mathcal{V} \oplus V_\mathcal{E}^{tol_\mathcal{E}} \oplus V_\mathcal{F}^{tol_\mathcal{F}};$$

see (9), (7), and (8) for a definition of $V_\mathcal{V}$, $V_\mathcal{E}^{tol_\mathcal{E}}$, and $V_\mathcal{F}^{tol_\mathcal{F}}$.

We construct the coarse interpolant $I_0$ from a point-wise interpolation

$$I_\mathcal{V} u := \sum_{v\in\mathcal{V}} u(v)\,\phi_v$$

to the space $V_\mathcal{V}$ and from the projections $\Pi_\mathcal{E}$ and $\Pi_\mathcal{F}$ onto the spaces spanned by the edge and face coarse basis functions, respectively; cf. (10) and (11). In particular, we define the coarse component of the stable decomposition as

$$u_0 := I_0 u := I_\mathcal{V} u + \Pi_\mathcal{E} u + \Pi_\mathcal{F} u.$$

The projection operators $I_\mathcal{V}$, $\Pi_\mathcal{E}$, and $\Pi_\mathcal{F}$ satisfy the following assumption:

Assumption 1. *As in Lemma 2, let $\xi$ be an open and connected interface component and $\Pi$ the corresponding projection operator. Then,*

$$z_{\xi\to\Omega_\xi}(\Pi_* v) = \Pi_* z_{\xi\to\Omega_\xi}(v) = 0 \quad \forall v \in V^h(\Omega)$$

*for any other projection operator $\Pi_* \ne \Pi$.*

This assumption is satisfied for the projection operators of the AGDSW coarse space interpolation. In particuar, we have

$$\begin{aligned} I_\mathcal{V} z_{e\to\Omega_e}(v) = z_{e\to\Omega_e}(I_\mathcal{V} v) = \Pi_\mathcal{F} z_{e\to\Omega_e}(v) = z_{e\to\Omega_e}(\Pi_\mathcal{F} v) = 0 \quad \forall v \in V^h(\Omega) \text{ and} \\ I_\mathcal{V} z_{f\to\Omega_f}(v) = z_{f\to\Omega_f}(I_\mathcal{V} v) = \Pi_\mathcal{E} z_{f\to\Omega_f}(v) = z_{f\to\Omega_f}(\Pi_\mathcal{E} v) = 0 \quad \forall v \in V^h(\Omega), \end{aligned}$$

which follows from the definition of $z_{e\to\Omega_e}(\cdot)$ and $z_{f\to\Omega_f}(\cdot)$, since vertex basis functions vanish on edges and faces, edge basis functions vanish on vertices and faces, and face basis functions vanish on vertices and edges.

To prove the existence of a stable decomposition, we first prove the following lemma. It states estimates for the edge and face functions that arise during the proof; cf. Theorem 6.

LEMMA 3. *Let the assumptions of Lemma 2 and Assumption 1 be satisfied, then*

$$|z_{\xi\to\Omega_\xi}(u-u_0)|^2_{a,\Omega_i} \leq |z_{\xi\to\Omega_\xi}(u-u_0)|^2_{a,\Omega_\xi} \leq \frac{C_{inv,\xi}}{tol_\xi}\sum_{k\in n^\xi}|u|^2_{a,\Omega_k}$$

*for an edge $\xi = e \in \mathcal{E}$ or a face $\xi = f \in \mathcal{F}$.*

*Proof.* Due to Assumption 1 we have on an edge $e$

$$\begin{aligned} z_{e\to\Omega_e}(u-u_0) &= z_{e\to\Omega_e}(u) - z_{e\to\Omega_e}\left(I_{\mathcal{V}}u + \Pi_{\mathcal{E}}u + \Pi_{\mathcal{F}}u\right) \\ &\overset{Asm.\ 1}{=} z_{e\to\Omega_e}(u) - z_{e\to\Omega_e}\left(\Pi_{\mathcal{E}}u\right) = z_{e\to\Omega_e}(u) - z_{e\to\Omega_e}\left(\Pi_e u\right) \\ &= z_{e\to\Omega_e}(u) - \Pi_e z_{e\to\Omega_e}(u) \end{aligned}$$

and, analogously, $z_{f\to\Omega_f}(u-u_0) = z_{f\to\Omega_f}(u) - \Pi_f z_{f\to\Omega_f}(u)$ on a face $f$. Therefore, using Lemma 2 we obtain

$$\begin{aligned} |z_{\xi\to\Omega_\xi}(u-u_0)|^2_{a,\Omega_i} &\leq |z_{\xi\to\Omega_\xi}(u-u_0)|^2_{a,\Omega_\xi} = |z_{\xi\to\Omega_\xi}(u) - \Pi_\xi z_{\xi\to\Omega_\xi}(u)|^2_{a,\Omega_\xi} \\ &\overset{Lemma\ 2}{\leq} \frac{C_{\text{inv},\xi}}{tol_\xi}\sum_{k\in n^\xi}|u|^2_{a,\Omega_k}. \end{aligned}$$

Next, we derive an estimate for the energy of the coarse component on a subdomain.

LEMMA 4. *Under the assumptions of Lemma 3, for $i \in \{1,\dots,N\}$, we have*

$$|u_0|^2_{a,\Omega_i} \leq 2\,|u|^2_{a,\Omega_i} + \frac{4N^e C_{\text{inv,e}}}{tol_{\mathcal{E}}}\sum_{e\subset\partial\Omega_i}\sum_{k\in n^e}|u|^2_{a,\Omega_k} + \frac{4N^f C_{\text{inv,f}}}{tol_{\mathcal{F}}}\sum_{f\subset\partial\Omega_i}\sum_{k\in n^f}|u|^2_{a,\Omega_k},$$

*where $N^e$ and $N^f$ denote the maximum number of edges and faces, respectively, a subdomain can have.*

*Proof.* We can use the fact that $u_0$ is discrete harmonic on each subdomain $\Omega_i$ and consider the contributions on the interface components separately. Since $u - u_0 = 0$ in the vertices, we obtain

$$\begin{aligned} |u_0|^2_{a,\Omega_i} &\leq 2\,|\mathcal{H}_{\partial\Omega_i\to\Omega_i}(u)|^2_{a,\Omega_i} + 2\,|\mathcal{H}_{\partial\Omega_i\to\Omega_i}(u-u_0)|^2_{a,\Omega_i} \\ &= 2(|\mathcal{H}_{\partial\Omega_i\to\Omega_i}(u)|^2_{a,\Omega_i} \\ &\quad + \Big|\sum_{e\subset\partial\Omega_i}\mathcal{H}_{\partial\Omega_i\to\Omega_i}\big(z_{e\to\partial\Omega_i}(u-u_0)\big) + \sum_{f\subset\partial\Omega_i}\mathcal{H}_{\partial\Omega_i\to\Omega_i}\big(z_{f\to\partial\Omega_i}(u-u_0)\big)\Big|^2_{a,\Omega_i}) \end{aligned}$$

Using a Cauchy-Schwarz inequality and the energy-minimality of $\mathcal{H}_{\partial\Omega_i\to\Omega_i}(\cdot)$ gives

$$\begin{aligned} |u_0|^2_{a,\Omega_i} \leq 2\,|u|^2_{a,\Omega_i} &+ 4N^e\sum_{e\subset\partial\Omega_i}\left|z_{e\to\Omega_e}(u-u_0)\right|^2_{a,\Omega_i} \\ &+ 4N^f\sum_{f\subset\partial\Omega_i}\left|z_{f\to\Omega_f}(u-u_0)\right|^2_{a,\Omega_i}, \end{aligned}$$

where $N^e$ and $N^f$ denote the maximum number of edges and faces, respectively, a subdomain can have. Finally, using Lemma 3, we obtain

$$|u_0|^2_{a,\Omega_i} \leq 2\,|u|^2_{a,\Omega_i} + \frac{4N^e C_{\text{inv,e}}}{tol_{\mathcal{E}}}\sum_{e\subset\partial\Omega_i}\sum_{k\in n^e}|u|^2_{a,\Omega_k} + \frac{4N^f C_{\text{inv,f}}}{tol_{\mathcal{F}}}\sum_{f\subset\partial\Omega_i}\sum_{k\in n^f}|u|^2_{a,\Omega_k}. \qquad \square$$

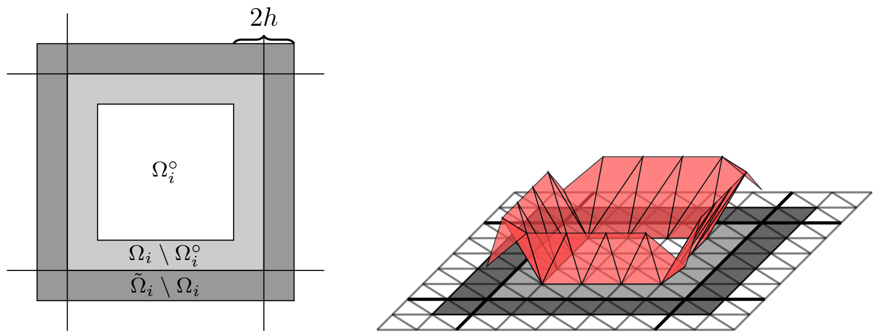


FIG. 4. *In the proof of Theorem 6, we consider a partition of unity corresponding to an overlapping decomposition $\{\tilde{\Omega}_i\}_{i=1}^N$ with overlap $h$. The corresponding regions $\Omega_i^\circ$ (white), $G_1 := \Omega_i \setminus \Omega_i^\circ$ (light gray), and $G_2 := \tilde{\Omega}_i \setminus \Omega_i$ (dark gray) are depicted in two dimensions (**left**). A finite element function $\psi$ on $G$ that is constant on the edges and vanishes on $\partial\Omega_i^\circ$ (**right**); cf. Lemma 5. Left figure from [24, Fig. 6.1].*

In Theorem 6, we prove the existence of a stable decomposition by introducing an overlapping decomposition $\{\tilde{\Omega}_i\}_{i=1}^N$ with overlap $h$ corresponding to the nonoverlapping decomposition $\{\Omega_i\}_{i=1}^N$; cf. Figure 4. Note that, in general, this decomposition differs from $\{\Omega_i'\}_{i=1}^N$, the one used in the first level of the preconditioner with overlap $\delta \geq h$. The decomposition $\{\tilde{\Omega}_i\}_{i=1}^N$ is only used in the proof and does not place any restriction on $\delta$. However, it does remove the dependence of the condition number estimate in Corollary 7 on the size of the overlap $\delta$.

In the proof of the stable decomposition, we need to estimate the energy of local components $I^h(\theta_i(u - u_0))$, given a partition of unity $\{\theta_i\}_{i=1}^N$ defined on the overlapping decomposition $\{\tilde{\Omega}_i\}_{i=1}^N$. The following lemma is used in Theorem 6 to estimate the energy of the local components on the overlap.

LEMMA 5. *Let the assumptions of Lemma 3 be satisfied. For any subdomain $\Omega_i$, $i \in \{1, \dots N\}$, let $G \subseteq \tilde{\Omega}_i \setminus \Omega_i^\circ$, where $\Omega_i^\circ$ denotes the non-overlapping subset of $\Omega_i$; cf. Figure 4. We consider a finite element function $\psi \in V^h(G)$ that can have arbitrary values on $\partial\Omega_i$ but vanishes on $\partial(\tilde{\Omega}_i \setminus \Omega_i^\circ) \cap \overline{G}$. Moreover, we assume that $0 \leq \psi \leq 1$, and that $\psi|_e$ and $\psi|_f$ are constant on $e \in \mathcal{E}$ and $f \in \mathcal{F}$, respectively. Then,*

$$\left| I^h\Big(\psi \cdot (u - u_0)\Big)\right|_{a,G}^2 \leq \frac{2N^e C_{\mathrm{inv,e}}}{tol_{\mathcal{E}}} \sum_{e \subset \partial\Omega_i} \sum_{k \in n^e} |u|_{a,\Omega_k}^2 + \frac{2N^f C_{\mathrm{inv,f}}}{tol_{\mathcal{F}}} \sum_{f \subset \partial\Omega_i} \sum_{k \in n^f} |u|_{a,\Omega_k}^2,$$

*where $N^e$ and $N^f$ correspond to the maximum number of edges and faces, respectively, a subdomain can have.*

Note that in the proof of the stable decomposition in Theorem 6, we will make use of Lemma 5 with the sets $G = G_1$ and $G = G_2$; cf. Figure 4.

*Proof.* We observe that $z_{e\to\Omega}(\cdot)$ and $z_{f\to\Omega}(\cdot)$ are identity operators on $e$ and $f$, respectively, and that $u - u_0$ vanishes in the vertices. Then, since $G_1 = \Omega_i \setminus \Omega_i^\circ$ and $G_2 = \tilde{\Omega}_i \setminus \Omega_i$ have width $1h$ and since $\psi$, $z_{e\to\Omega_e}$, and $z_{f\to\Omega_f}$ all vanish on $\partial(\tilde{\Omega}_i \setminus \Omega_i^\circ) \cap \overline{G}$, we have with $\psi_0 := \psi \cdot (u - u_0)$

$$\begin{aligned}\left|I^h(\psi_0)\right|_{a,G}^2 &= \Big| \sum_{e \subset \partial\Omega_i} z_{e\to\Omega}(\psi_0) + \sum_{f \subset \partial\Omega_i} z_{f\to\Omega}(\psi_0)\Big|_{a,G}^2 \\ &\leq 2\Big| \sum_{e \subset \partial\Omega_i} z_{e\to\Omega}(\psi_0)\Big|_{a,G}^2 + 2\Big| \sum_{f \subset \partial\Omega_i} z_{f\to\Omega}(\psi_0)\Big|_{a,G}^2.\end{aligned}$$

Then, a Cauchy-Schwarz inequality, the fact that $\psi|_e$ is constant and that $0 \leq \psi \leq 1$, gives

$$\Big| \sum_{e \subset \partial\Omega_i} z_{e \to \Omega}\Big(\psi\,(u-u_0)\Big)\Big|^2_{a,G} \leq N^e \sum_{e \subset \partial\Omega_i} \Big| z_{e \to \Omega}\Big(\psi\,(u-u_0)\Big)\Big|^2_{a,G}$$
$$\leq N^e \sum_{e \subset \partial\Omega_i} \left(\psi|_e\right)^2 \left|z_{e\to\Omega}\,(u-u_0)\right|^2_{a,G} \leq N^e \sum_{e \subset \partial\Omega_i} \left|z_{e\to\Omega}\,(u-u_0)\right|^2_{a,G}.$$

Finally, using Lemma 3, we obtain

$$\sum_{e \subset \partial\Omega_i} \left|z_{e\to\Omega}\,(u-u_0)\right|^2_{a,G} \leq \sum_{e \subset \partial\Omega_i} \left|z_{e\to\Omega}\,(u-u_0)\right|^2_{a,\Omega_e} \leq \frac{C_{\text{inv,e}}}{tol_{\mathcal{E}}} \sum_{e \subset \partial\Omega_i} \sum_{k \in n^e} |u|^2_{a,\Omega_k}.$$

Completely analogously, using Lemma 3, we have

$$\Big| \sum_{f \subset \partial\Omega_i} z_{f \to \Omega}\Big(\psi\,(u-u_0)\Big)\Big|^2_{a,G} \leq \frac{N^f C_{\text{inv,f}}}{tol_{\mathcal{F}}} \sum_{f \subset \partial\Omega_i} \sum_{k \in n^f} |u|^2_{a,\Omega_k}.$$

Therefore,

$$\left|I^h(\psi_0)\right|^2_{a,G} \leq 2\Big|\sum_{e \subset \partial\Omega_i} z_{e\to\Omega}(\psi_0)\Big|^2_{a,G} + 2\Big|\sum_{f \subset \partial\Omega_i} z_{f\to\Omega}(\psi_0)\Big|^2_{a,G}$$
$$\leq \frac{2N^e C_{\text{inv,e}}}{tol_{\mathcal{E}}} \sum_{e \subset \partial\Omega_i} \sum_{k \in n^e} |u|^2_{a,\Omega_k} + \frac{2N^f C_{\text{inv,f}}}{tol_{\mathcal{F}}} \sum_{f \subset \partial\Omega_i} \sum_{k \in n^f} |u|^2_{a,\Omega_k}. \qquad \square$$

Now, we are able to prove the existence of a stable decomposition.

THEOREM 6 (Stable Decomposition). *Under the assumptions of Lemma 3, for each $u \in V^h(\Omega)$, there exists a decomposition $u = \sum_{i=0}^{N} R_i^T u_i$, $u_i \in V_i = V^h(\Omega_i')$, where $\Omega_0' := \Omega$, such that*

$$\sum_{i=0}^{N} |u_i|^2_{a,\Omega_i'} \leq C_0^2\, |u|^2_{a,\Omega},$$

*where $C_0^2 = \left(20 + \frac{34(N^e)^2 n^e_{max} C_{\text{inv,e}}}{tol_{\mathcal{E}}} + \frac{68(N^f)^2 C_{\text{inv,f}}}{tol_{\mathcal{F}}}\right)$ and $N^e$ and $N^f$ correspond to the maximum number of edges and faces, respectively, a subdomain can have, and $n^e_{max}$ corresponds to the maximum number of adjacent subdomains an edge can have.*

*Proof.* On the overlapping decomposition $\{\tilde{\Omega}_i\}_{i=1}^N$ of width $1h$, we consider the local components $u_i := I^h\left(\theta_i\,(u-u_0)\right)$ with the partition of unity $\{\theta_i\}_{i=1}^N$, $\theta_i \in V^h(\Omega)$, where

$$\theta_i(x^h) := \begin{cases} \frac{1}{|n^e|} & \text{on edges } e \in \mathcal{E}, \\ \frac{1}{|n^f|} & \text{on faces } f \in \mathcal{F}, \\ \frac{1}{|n^v|} & \text{on vertices } v \in \mathcal{V}, \\ 1 & \text{in } \Omega_i^\circ, \\ 0 & \text{elsewhere,} \end{cases}$$

where $x^h$ is a finite element node and where $\Omega_i^\circ$ denotes the non-overlapping subset of $\tilde{\Omega}_i$; cf. Figure 4. Note that, since $\tilde{\Omega}_i \subset \Omega_i'$, we still have $u_i \in V_i$. We consider the partition

$$\tilde{\Omega}_i = (\tilde{\Omega}_i \setminus \Omega_i) \cup (\Omega_i \setminus \Omega_i^\circ) \cup \Omega_i^\circ.$$

Therefore, we have

$$|u_i|^2_{a,\tilde{\Omega}_i} = |u_i|^2_{a,\tilde{\Omega}_i \setminus \Omega_i} + |u_i|^2_{a,\Omega_i \setminus \Omega_i^\circ} + |u_i|^2_{a,\Omega_i^\circ} . \tag{15}$$

To proceed, we use the estimate for $|u_0|^2_{a,\Omega_i}$ from Lemma 4. Let

$$Z_{\mathcal{E}} := \frac{4N^e C_{\text{inv,e}}}{tol_{\mathcal{E}}} \sum_{e \subset \partial\Omega_i} \sum_{k \in n^e} |u|^2_{a,\Omega_k} , \qquad Z_{\mathcal{F}} := \frac{4N^f C_{\text{inv,f}}}{tol_{\mathcal{F}}} \sum_{f \subset \partial\Omega_i} \sum_{k \in n^f} |u|^2_{a,\Omega_k} ,$$

then we have for the last additive term in (15)

$$\begin{aligned}
|u_i|^2_{a,\Omega_i^\circ} &= \left|I^h\big(\theta_i(u-u_0)\big)\right|^2_{a,\Omega_i^\circ} = |u-u_0|^2_{a,\Omega_i^\circ} \le |u-u_0|^2_{a,\Omega_i} \\
&\le 2\,|u|^2_{a,\Omega_i} + 2\,|u_0|^2_{a,\Omega_i} \overset{\text{Lemma 4}}{\le} 2\,|u|^2_{a,\Omega_i} + 2\left(2\,|u|^2_{a,\Omega_i} + Z_{\mathcal{E}} + Z_{\mathcal{F}}\right) \\
&= 6\,|u|^2_{a,\Omega_i} + 2Z_{\mathcal{E}} + 2Z_{\mathcal{F}}. \qquad (16)
\end{aligned}$$

Furthermore, we have for the second additive term in (15)

$$\begin{aligned}
|u_i|^2_{a,\Omega_i \setminus \Omega_i^\circ} &\le 2\,|u_i - (u-u_0)|^2_{a,\Omega_i \setminus \Omega_i^\circ} + 2\,|u-u_0|^2_{a,\Omega_i \setminus \Omega_i^\circ} \\
&\le 2\left|I^h((1-\theta_i)\,(u-u_0)\right|^2_{a,\Omega_i \setminus \Omega_i^\circ} + 2\,|u-u_0|^2_{a,\Omega_i} . \qquad (17)
\end{aligned}$$

We observe that, on an edge $e \in \mathcal{E}$ or a face $f \in \mathcal{F}$, the restrictions of $\theta_i$ are constant according to its definition:

$$\theta_i|_e = \frac{1}{|n^e|} \le \frac{1}{2}, \quad \theta_i|_f = \frac{1}{|n^f|} = \frac{1}{2}.$$

Therefore, setting $\psi := 1 - \theta_i$ and $G := G_1 = \Omega_i \setminus \Omega_i^\circ$, we can use Lemma 5 to bound the first additive term of equation (17). Note that we cannot set $\psi = \theta_i$ to derive an estimate for $|u_i|^2_{a,\Omega_i \setminus \Omega_i^\circ}$ directly, since Lemma 5 requires $\psi = 0$ on the boundary of $\Omega_i^\circ$. Using Lemma 4 and equation (16), we obtain for equation (17)

$$\begin{aligned}
|u_i|^2_{a,\Omega_i \setminus \Omega_i^\circ} &\le 2\left|I^h\big((1-\theta_i)\,(u-u_0)\,\big)\right|^2_{a,\Omega_i \setminus \Omega_i^\circ} + 2\,|u-u_0|^2_{a,\Omega_i} \\
&\le 2\Big(0.5Z_{\mathcal{E}} + 0.5Z_{\mathcal{F}}\Big) + 2\Big(6\,|u|^2_{a,\Omega_i} + 2Z_{\mathcal{E}} + 2Z_{\mathcal{F}}\Big) \\
&= 12\,|u|^2_{a,\Omega_i} + 5Z_{\mathcal{E}} + 5Z_{\mathcal{F}}. \qquad (18)
\end{aligned}$$

Now, setting $\psi := \theta_i$ on $G := G_2 = \tilde{\Omega}_i \setminus \Omega_i$ and using Lemma 5, we have

$$|u_i|^2_{a,\tilde{\Omega}_i \setminus \Omega_i} = \left|I^h\Big(\theta_i(u-u_0)\Big)\right|^2_{a,\tilde{\Omega}_i \setminus \Omega_i} \le 0.5Z_{\mathcal{E}} + 0.5Z_{\mathcal{F}}. \tag{19}$$

Summing the edge and face contributions $Z_{\mathcal{E}}$ and $Z_{\mathcal{F}}$ over all subdomains, we obtain

$$\begin{aligned}
\sum_{i=1}^N (Z_{\mathcal{E}} + Z_{\mathcal{F}}) &= \sum_{i=1}^N 4\left(\frac{N^e C_{\text{inv,e}}}{tol_{\mathcal{E}}} \sum_{e \subset \partial\Omega_i} \sum_{k \in n^e} |u|^2_{a,\Omega_k} + \frac{N^f C_{\text{inv,f}}}{tol_{\mathcal{F}}} \sum_{f \subset \partial\Omega_i} \sum_{k \in n^f} |u|^2_{a,\Omega_k}\right) \\
&\le \frac{4(N^e)^2 n^e_{\max} C_{\text{inv,e}}}{tol_{\mathcal{E}}} |u|^2_{a,\Omega} + \frac{4(N^f)^2 2 C_{\text{inv,f}}}{tol_{\mathcal{F}}} |u|^2_{a,\Omega}, \qquad (20)
\end{aligned}$$

where $n^e_{\max}$ corresponds to the maximum number of adjacent subdomains of an edge. Finally, using

$$|u_0|^2_{a,\Omega} = \sum_{i=1}^N |u_0|^2_{a,\Omega_i} ,$$

we obtain with Lemma 4 and equations (16), (18), (19), and (20)

$$\begin{aligned}\sum_{i=0}^{N} |u_i|^2_{a,\Omega} &= \sum_{i=1}^{N} \left( |u_0|^2_{a,\Omega_i} + |u_i|^2_{a,\tilde{\Omega}_i \setminus \Omega_i} + |u_i|^2_{a,\Omega_i \setminus \Omega_i^\circ} + |u_i|^2_{a,\Omega_i^\circ} \right) \\ &\leq \sum_{i=1}^{N} \left( 20\, |u|^2_{a,\Omega_i} + 8.5 Z_{\mathcal{E}} + 8.5 Z_{\mathcal{F}} \right) \\ &\leq \left( 20 + \frac{34 (N^e)^2 n^e_{\max} C_{\text{inv,e}}}{tol_{\mathcal{E}}} + \frac{68 (N^f)^2 C_{\text{inv,f}}}{tol_{\mathcal{F}}} \right) |u|^2_{a,\Omega}\,. \qquad \square\end{aligned}$$

From Theorem 6, we directly obtain a condition number estimate for the preconditioned system.

Corollary 7. *The condition number of the AGDSW two level Schwarz operator in three dimensions is bounded by*

$$\kappa \left( M^{-1}_{\text{AGDSW}} K \right) \leq \left( 20 + \frac{34 (N^e)^2 n^e_{max}}{tol_{\mathcal{E}}} + \frac{68 (N^f)^2}{tol_{\mathcal{F}}} \right) \left( \hat{N}_c + 1 \right).$$

*The constant $\hat{N}_c$ is an upper bound for the number of overlapping subdomains each point $x \in \Omega$ can belong to. All constants are independent of $H$, $h$, and the contrast of the coefficient function $A$.*

*Proof.* Since we use exact local solvers, we directly obtain

$$\kappa \left( M^{-1}_{\text{AGDSW}} K \right) \leq C_0^2 \left( \hat{N}_c + 1 \right),$$

where $C_0^2$ is the constant of the stable decomposition; cf. [53, Lemma 3.11] and the follow-up discussion and the proof of [13, Theorem 4.1]. We obtain the final estimate using Theorem 6 and $C_{\text{inv,e}} = C_{\text{inv,f}} = 1$; cf. Remark 3. $\square$

Remark 4. *The proof for the two-dimensional case can be performed analogously to the three-dimensional case. In particular, the edges in two dimensions can be handled in the same way as the faces in three dimensions. For the AGDSW two level Schwarz operator, we obtain the condition number bound*

$$\kappa \left( M^{-1}_{\text{AGDSW}} K \right) \leq \left( 20 + \frac{68 (N^e)^2}{tol_{\mathcal{E}}} \right) \left( \hat{N}_c + 1 \right).$$

**7. Variants of adaptive GDSW.** There are several modifications that can be applied to the AGDSW coarse space. First, the right hand side of the eigenvalue problem can be replaced by a bilinear form that corresponds to a scaled $L^2$-inner product or a scaled mass matrix, respectively; cf. subsection 7.1. To the best of our knowledge, this modification does not lead to an advantage, since the mass matrix has to be additionally assembled whereas the stiffness matrices in an implementation of the right hand side of the eigenvalue problem (5) can be extracted directly from the fully assembled global stiffness matrix $K$. However, it shows the connection of the AGDSW coarse space to other related coarse spaces, e.g., the OS-ACMS, SHEM, wirebasket, and vertex-based coarse spaces; see [24, 19, 16]. Second, a parallel implementation of the left hand side of the eigenvalue problem (5) is facilitated and the computational cost is reduced by using a sum of local, decoupled parts that can then be computed independently; cf. subsection 7.2. A third modification can be used to further decrease the work for the computation of the left hand side of the eigenvalue problem. Here, we consider discrete harmonic extensions onto slabs of finite elements instead of the union of all subdomains which are adjacent to the corresponding edge or face; cf. subsection 7.3.

Remark 5. *The standard AGDSW algorithm and the mentioned modifications above can also be used in two dimensions, see [23], in which the edge basis functions were constructed slightly differently. The construction presented in subsection 5.1 significantly simplifies the setup of the generalized eigenvalue problems, reduces the computational cost, and can decrease the coarse space dimension.*

**7.1. Mass matrix.** As in other adaptive coarse spaces, where the generalized eigenvalue problem is used to replace a Poincaré type inequality, cf., e.g. [17, 14, 12], we can use a scaled mass matrix on the right hand side of the eigenvalue problems (5) as well. Let $\xi$ be an edge $e \in \mathcal{E}$ or a face $f \in \mathcal{F}$, then the scaled mass matrix corresponding to the edge $e$ or face $f$ arises from the discretization of the scaled $L^2$-inner product

$$b_\xi\left(u, v\right) := \frac{1}{h^2}\left(A\, z_{\xi\to\Omega_\xi}(u), z_{\xi\to\Omega_\xi}(v)\right)_{L^2(\Omega_\xi)}.$$

The corresponding norm is defined as

$$\|v\|_{b,\xi}^2 := b_\xi\left(v, v\right).$$

Therefore, we obtain for the generalized eigenvalue problem: find $\tau_{*,\xi} \in V_0^h\left(\xi\right)$, s.t.

$$a_{\Omega_\xi}\left(\mathcal{H}_{\xi\to\Omega_\xi}(\tau_{*,\xi}), \mathcal{H}_{\xi\to\Omega_\xi}(\theta)\right) = \lambda_{*,\xi} b_\xi\left(\tau_{*,\xi}, \theta\right) \quad \forall \theta \in V_0^h\left(\xi\right).$$

We denote the resulting coarse space by $V_{\mathrm{AGDSW-M}}$. For $v \in V^h(\xi)$, we have

$$\left|z_{\xi\to\Omega_\xi}(v)\right|_{a,\Omega_\xi}^2 = \int_{\Omega_\xi} A\left(\nabla z_{\xi\to\Omega_\xi}(v)\right)^2 dx \le \frac{C_{\mathrm{inv}}}{h^2}\int_{\Omega_\xi} A\, z_{\xi\to\Omega_\xi}(v)^2\, dx = b_\xi(v, v),$$

since $A$ is constant on each fine element $T \in \tau_h(\Omega)$. The constant $C_{\mathrm{inv}} > 0$ arises from the use of an inverse equality on the elements. It is independent of $H$, $h$, and the contrast of the coefficient function.

Remark 6. *The constant $C_{\mathrm{inv}}$ depends only on the shape parameter of the triangulation and the polynomial degree of the shape functions; see, e.g., [54, Section 3.6], where also a concrete upper bound for $C_{\mathrm{inv}}$ is given.*

We obtain a condition number bound analogously to Corollary 7 by setting $c(\cdot,\cdot) := b_\xi(\cdot,\cdot)$ in Lemma 2.

Corollary 8. *The condition number of the AGDSW-M two level Schwarz operator in three dimensions is bounded by*

$$\kappa\left(M_{\mathrm{AGDSW-M}}^{-1}K\right) \le \left(20 + 34C_{\mathrm{inv}}\left(\frac{(N^e)^2 n_{max}^e}{tol_{\mathcal{E}}} + \frac{2(N^f)^2}{tol_{\mathcal{F}}}\right)\right)\left(\hat{N}_c + 1\right).$$

*All constants are independent of $H$, $h$, and the contrast of the coefficient function.*

Remark 7. *If the mesh regularity or uniformity is low, better numerical results may be achieved by scaling element-wise with the radius of the largest insphere, i.e., let $r_s$ be a function that is constant on each finite element $T \in \tau_h(\Omega)$, on which it assumes the radius of the largest insphere of $T$. Then, we define on an edge $\xi = e \in \mathcal{E}$ or a face $\xi = f \in \mathcal{F}$*

$$b_\xi(u, v) := \left(\frac{A}{r_s^2} z_{\xi\to\Omega_\xi}(u), z_{\xi\to\Omega_\xi}(v)\right)_{L^2(\Omega_\xi)}.$$

**7.2. Local Neumann problems.** In a parallel implementation of the generalized face eigenvalue problem (5) we can utilize the fact that the discrete harmonic extension is only weakly coupled via the boundary nodes of the face. Thus, instead of computing the (coupled) extension simultaneously to both subdomains adjacent to the face, we can compute extensions independently to each adjacent subdomain without losing much information. The same holds in two dimensions for the edge eigenvalue problems. Similarly, in three dimensions for edges, we can compute the discrete harmonic extensions independently to the adjacent subdomains. However, the stronger the coupling between the subdomains, the more information is lost, which can result in an increased coarse space dimension.

Let either $\xi = e \in \mathcal{E}$ or $\xi = f \in \mathcal{F}$, then

$$a_{\Omega_\xi}\left(\mathcal{H}_{\xi\to\Omega_\xi}(\tau_{*,\xi}), \mathcal{H}_{\xi\to\Omega_\xi}(\theta)\right) \neq \sum_{k\in n^\xi} a_{\Omega_k}\left(\mathcal{H}_{\xi\to\Omega_k}(\tau_{*,\xi}), \mathcal{H}_{\xi\to\Omega_k}(\theta)\right).$$

Nevertheless, we can replace the left hand side of the eigenvalue problem by the sum of the local contributions and obtain the eigenvalue problems: find $\tau_{*,\xi} \in V_0^h(\xi)$ s.t.

$$\sum_{k\in n^\xi} a_{\Omega_k}\left(\mathcal{H}_{\xi\to\Omega_k}(\tau_{*,\xi}), \mathcal{H}_{\xi\to\Omega_k}(\theta)\right) = \lambda_{*,\xi} a_{\Omega_\xi}\left(z_{\xi\to\Omega_\xi}(\tau_{*,\xi}), z_{\xi\to\Omega_\xi}(\theta)\right) \quad \forall \theta \in V_0^h(\xi).$$

We denote the resulting coarse space by $V_{\text{AGDSW-S}}$. Using these modified eigenvalue problems yields the same condition number estimate as in Corollary 7.

Corollary 9. *The condition number of the AGDSW-S two level Schwarz operator in three dimensions is bounded by*

$$\kappa\left(M_{\text{AGDSW-S}}^{-1}K\right) \leq \left(20 + \frac{34(N^e)^2 n^e_{max}}{tol_{\mathcal{E}}} + \frac{68(N^f)^2}{tol_{\mathcal{F}}}\right)\left(\hat{N}_c + 1\right).$$

*All constants are independent of $H$, $h$, and the contrast of the coefficient function $A$.*

*Proof.* We only have to show that the assumptions of Lemma 2 are satisfied. Then, the proof is exactly the same as for Corollary 7.

The bilinear form $d(\cdot,\cdot) := \sum_{k\in n^\xi} a_{\Omega_k}\left(\mathcal{H}_{\xi\to\Omega_k}(\cdot), \mathcal{H}_{\xi\to\Omega_k}(\cdot)\right)$ is symmetric and positiv semi-definite and satisfies

$$d(v,v) = \sum_{k\in n^\xi} |\mathcal{H}_{\xi\to\Omega_k}(v)|^2_{a,\Omega_k} \leq \sum_{k\in n^\xi} |v|^2_{a,\Omega_k} = |v|^2_{a,\Omega_\xi} \quad \forall v \in V^h(\xi).$$

∎

As we are going to observe, this variant of AGDSW can lead to a slightly larger coarse space. However, the implementation and computation of the eigenvalue problems is simplified.

**7.3. Economic version using slabs.** In order to reduce the computational cost of the computation of the eigenvalue problems, the size of the sets $\Omega_e$ and $\Omega_f$ can be reduced. In particular, we propose a variant where slabs of width $l$ elements around the edges or faces are used instead of complete subdomains; cf. Figure 5 for the graphical representation of the slabs. We denote these slabs by $\Omega_e^l$ and $\Omega_f^l$. The idea of computing the Schur complement only on slabs of minimal width was initially proposed in [10]. It was then applied to eigenvalue problems and more general slabs in [38]. Finally, in [24], a multiscale coarse space based on the ACMS space was introduced for which an economic variant on slabs was proposed.

The modified eigenvalue problem reads for an edge $\xi = e \in \mathcal{E}$ or a face $\xi = f \in \mathcal{F}$: find $\tau_{*,\xi} \in V_0^h(\xi)$ such that

$$a_{\Omega_\xi^l}\left(\mathcal{H}_{\xi\to\Omega_\xi^l}(\tau_{*,\xi}), \mathcal{H}_{\xi\to\Omega_\xi^l}(\theta)\right) = \lambda_{*,\xi} a_{\Omega_\xi}\left(z_{\xi\to\Omega_\xi}(\tau_{*,\xi}), z_{\xi\to\Omega_\xi}(\theta)\right) \quad \forall \theta \in V_0^h(\xi).$$

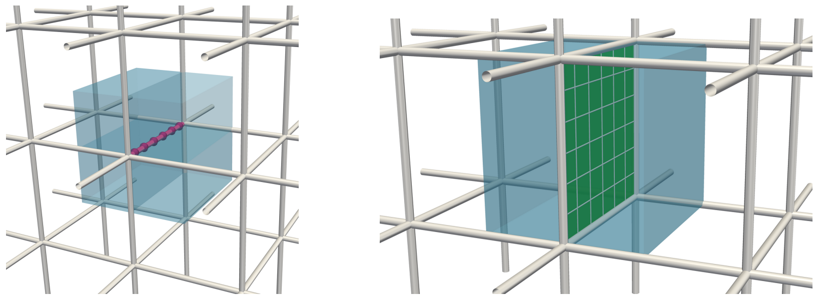

Fig. 5. *Three-dimensional version of the slab $\Omega_e^l$ corresponding to an edge (**left**) and a graphical representation of the slab $\Omega_f^l$ corresponding to the face $f$ (**right**).*

The slab variant is computationally cheaper and can be proven analogously to the standard version with no modifications. However, as for the variant with local Neumann problems, the coarse space dimension can be larger.

**8. Implementation remarks.** The classical GDSW coarse space can be implemented algebraically. However, the new coarse space $V_{\mathrm{AGDSW}}$ and the variant $V_{\mathrm{AGDSW-S}}$ require the local subdomain stiffness matrices, which cannot be extracted from the global stiffness matrix $K$. On the other hand, the matrix in the right hand side of the generalized eigenvalue problem (5) can be extracted from the fully assembled stiffness matrix $K$. Except for the slab variant, the matrix in the left hand side of the generalized eigenvalue problem (5) can be easily computed from the local (non-overlapping) stiffness matrices. For the slab variant, stiffness matrices on slabs need to be assembled. In the variant with local Neumann problems, $V_{\mathrm{AGDSW-S}}$, the implementation is further simplified, since the discrete harmonic extensions are then local to the subdomains and can be computed in parallel. Furthermore, numerical results suggest that GDSW and the adaptive variant only require a simple interface partitioning (components can be disconnected), which facilitates the implementation.

In [28, 27, 26], a parallel implementation of GDSW was considered for various model problems. In a future parallel implementation of AGDSW, we expect the setup of the generalized eigenvalue problems to be the bottleneck. Note that in [24] the inexact solution of the related generalized eigenvalue problems using LobPCG [42] was successful.

**9. Numerical results.** We present numerical results for the discretized variational problem (1), $f \equiv 1$, and several coefficient functions. Except for the test case in Figure 9 and Table 4, the computational domain is always the unit cube with a zero Dirichlet condition prescribed on its boundary.

We discretize (1) using piecewise trilinear basis functions on voxels or piecewise linear basis functions on tetrahedra and solve the resulting linear system with the preconditioned conjugate gradient (PCG) method and a relative stopping criterion $\|r^{(k)}\|_2/\|r^{(0)}\|_2 < 10^{-8}$, where $r^{(0)}$ and $r^{(k)}$ are the initial and the $k$-th unpreconditioned residuals. The reported condition number is the estimate obtained during the last iteration of the PCG method using the Lanczos method [49, ch. 6.7.3].

In the case of voxels, we always consider a cubic domain that is partitioned into smaller cubes. As for tetrahedra, we always partition the domain into subdomains using METIS [34].

We consider the adaptive coarse spaces based on GDSW and the vertex-based and wirebasket coarse spaces by Eikeland, Marcinkowski, and Rahman in [16].

By $V_{\mathrm{GDSW}}$ and $V_{\mathrm{AGDSW}}^{tol_{\mathcal{E}},tol_{\mathcal{F}}}$ we denote the GDSW and adaptive GDSW coarse spaces, respectively. Note that $V_{\mathrm{AGDSW}}^{0,0} = V_{\mathrm{GDSW}}$. The variant, which uses a

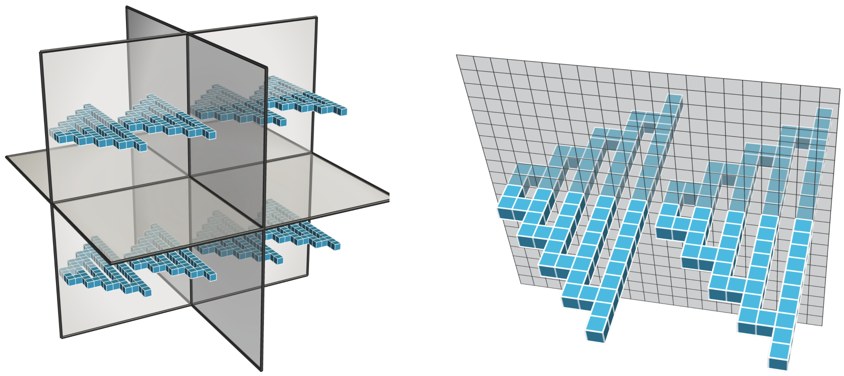

FIG. 6. *Discontinuous coefficient function $A$ with coefficients intersecting faces. The blue color corresponds to a coefficient of $A_{\max} = 10^6$ and the remainder is set to $A_{\min} = 1.0$. The left image shows the coefficient function for $2^3$ subdomains. One face is highlighted in the right image. The computational domain is a cube discretized using trilinear elements; $1/H = 2$; $H/h = 21$; $\delta = 1h$.*

| | Coefficient function $A$ from Figure 7 | | | |
|---|---|---|---|---|
| $V_0$ | $\mathcal{F}$ slab width $w$ | it. | $\kappa$ | $\dim V_0$ ($\mathcal{V}$,$\mathcal{E}$,$\mathcal{F}$) |
| $V_{\text{AGDSW}}$ | $1h$ | 51 | 30.7 | 55 (1,6,48) |
| $V_{\text{AGDSW}}$ | $2h$ | 45 | 32.7 | 47 (1,6,40) |
| $V_{\text{AGDSW}}$ | $4h$ | 45 | 32.6 | 39 (1,6,32) |
| $V_{\text{AGDSW}}$ | $6h$ | 49 | 32.6 | 31 (1,6,24) |
| $V_{\text{AGDSW}}$ | $8h$ | 51 | 32.6 | 23 (1,6,16) |
| $V_{\text{AGDSW}}$ | $21h$ | 51 | 32.6 | 23 (1,6,16) |
| $V_{\text{VB}}$ | – | 47 | 30.2 | 49 (1,0,48) |

TABLE 1

*Results for the coefficient function in Figure 6: slab width, iteration counts, condition number, and resulting coarse space dimension for different coarse spaces. A tolerance for the selection of the eigenfunctions of $10^{-2}$ was used for $V_{\text{AGDSW}}$ and $10^{-3}$ for $V_{\text{VB}}$. The full slab width was used for the edge eigenvalue problems of $V_{\text{AGDSW}}$. $1/H = 2$, $H/h = 21$, and $\delta = 1h$; maximum coefficient $A_{\max} = 10^6$; relative stopping criterion $\|r^{(k)}\|_2/\|r^{(0)}\|_2 < 10^{-8}$.*

scaled mass matrix in the right hand side of the eigenvalue problem is denoted by $V^{tol}_{\text{AGDSW-M}}$; see subsection 7.1. The variant using the sum of local Neumann problems on the left hand side of the eigenvalue problem is denoted by $V^{tol}_{\text{AGDSW-S}}$; see subsection 7.2. If not mentioned otherwise, the full slab (i.e., the union of subdomains which are adjacent to an edge or face) is used; see also subsection 7.3. By $V^{tol_{\mathcal{E}},tol_{\mathcal{F}}}_{\text{VB}}$ and $V^{tol_{\mathcal{E}},tol_{\mathcal{F}}}_{\text{WB}}$ we denote the vertex-based and wirebasket coarse spaces from [16].

We begin by showing results for $V_{\text{AGDSW}}$ and two coefficient functions by varying the width of the slab in order to highlight the effect of the harmonic extensions in the generalized eigenvalue problems of adaptive GDSW; the same behavior can be observed for the OS-ACMS coarse space introduced in [24]. We then show results for some realistic coefficient functions and, finally, some averaged results for random coefficient functions.

**9.1. Varying slab widths.** In this section, we investigate the effect of varying slab widths for $V_{\text{AGDSW}}$; cf. subsection 7.3. Instead of employing the discrete harmonic extensions in the eigenvalue problems on the union of the adjacent subdomains (of an edge or face), we restrict it to a slab around the edge or face. An advantage of using small slabs is the reduced computational cost of computing the discrete harmonic extension. However, we then weaken the detection of connected high coefficient components. The smaller the slab, the fewer connections can be detected.

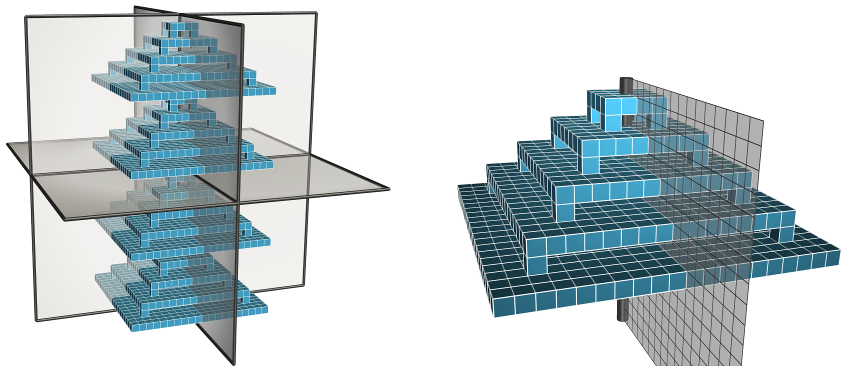

Fig. 7. *Discontinuous coefficient function $A$ with coefficients intersecting edges and faces. The blue color corresponds to a coefficient of $A_{\max} = 10^6$ and the remainder is set to $A_{\min} = 1.0$. The left image shows the coefficient function for $2^3$ subdomains; each vertical edge is intersected by two high-coefficient connected components. One such component, its corresponding edge, and one adjacent face are highlighted in the right image. The computational domain is a cube discretized using trilinear elements; $1/H = 2$; $H/h = 21$; $\delta = 1h$.*

| | Coefficient function $A$ from Figure 7 | | | |
|---|---|---|---|---|
| $V_0$ | $\mathcal{E}$ slab width $w$ | it. | $\kappa$ | $\dim V_0$ ($\mathcal{V}$,$\mathcal{E}$,$\mathcal{F}$) |
| $V_{\text{AGDSW}}$ | $1h$ | 71 | 125.5 | 45 (1,24,20) |
| $V_{\text{AGDSW}}$ | $2h$ | 71 | 125.5 | 41 (1,20,20) |
| $V_{\text{AGDSW}}$ | $4h$ | 70 | 125.5 | 37 (1,16,20) |
| $V_{\text{AGDSW}}$ | $6h$ | 70 | 125.6 | 33 (1,12,20) |
| $V_{\text{AGDSW}}$ | $8h$ | 69 | 125.7 | 29 (1, 8,20) |
| $V_{\text{AGDSW}}$ | $21h$ | 69 | 125.7 | 29 (1, 8,20) |
| $V_{\text{VB}}$ | – | 43 | 37.9 | 105 (1,20,84) |

Table 2

*Results for the coefficient function in Figure 7: slab width, iteration counts, condition number, and resulting coarse space dimension for different coarse spaces. A tolerance for the selection of the eigenfunctions of $10^{-2}$ was used for $V_{\text{AGDSW}}$ and $10^{-3}$ for $V_{\text{VB}}$. The full slab width was used for the face eigenvalue problems of $V_{\text{AGDSW}}$. $1/H = 2$, $H/h = 21$, and $\delta = 1h$; maximum coefficient $A_{\max} = 10^6$; relative stopping criterion $||r^{(k)}||_2/||r^{(0)}||_2 < 10^{-8}$.*

Therefore, we consider the coefficient function in Figure 6, where high coeffcient components intersect faces. The results for various slab widths are listed in Table 1. As can be seen, an increasing slab width yields a decreasing coarse space dimension, since fewer face eigenfunctions are required. A slab of width $8h$ covering the complete high coefficient component is sufficient to yield the same result as for the maximum width of $21h$ (in which case the slab is equal to the union of the adjacent subdomains).

Next, we consider an example for edges; see Figure 7. The numerical results in Table 2 show that using larger slabs in the edge eigenvalue problem reduced the number of edge eigenfunctions. For a slab width of $1h$ a total of 24 edge functions are included in $V_{\text{AGDSW}}$. This number reduces to a minimum of 8 edge functions for a slab width of $8h$.

We conclude that, for certain coefficient functions, the inclusion of the discrete harmonic extension in the eigenvalue problem can significantly reduce the coarse space dimension.

**9.2. Realistic and random coefficient functions.** In the following, we consider three coefficient functions which exhibit structures that are more likely to be encountered in realistic applications.

Figure 8 depicts 100 beams of high coefficients intersecting a cube that is partitioned into 125 subdomains. As is evident from Table 3 the classical GDSW method

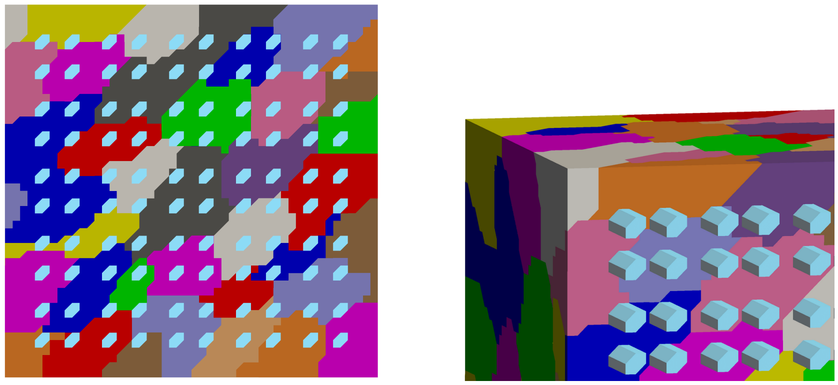

FIG. 8. *Cross section* (**left**) *of a domain decomposition of a cube and a discontinuous coefficient function $A$ with beams of high coefficients (light blue) crossing the domain. The beams of high coefficients do not touch the domain boundary. The light blue color corresponds to a coefficient of $A_{\max} = 10^6$ and the remainder is set to $A_{\min} = 1.0$. Number of subdomains: 125; number of nodes: 132 651; $\delta = 1h$. Structured tetrahedral mesh; unstructured domain decomposition (METIS).*

| | Coefficient function $A$ from Figure 8 | | | | | |
|---|---|---|---|---|---|---|
| $V_0$ | $tol_{\mathcal{E}}$ | $tol_{\mathcal{F}}$ | it. | $\kappa$ | $\dim V_0$ $(\mathcal{V},\mathcal{E},\mathcal{F})$ | $\dim V_0/\mathrm{dof}$ |
| $V_{\mathrm{GDSW}}$ | – | – | 1 060 | 467 954.2 | 1 987 (564, 790, 633) | 1.50% |
| $V_{\mathrm{AGDSW}}$ | $10^{-2}$ | $10^{-2}$ | 60 | 25.1 | 2 763 (564, 881, 1 318) | 2.08% |
| $V_{\mathrm{AGDSW-S}}$ | $10^{-2}$ | $10^{-2}$ | 60 | 25.1 | 2 763 (564, 881, 1 318) | 2.08% |
| $V_{\mathrm{AGDSW-M}}$ | $10^{-3}$ | $10^{-3}$ | 60 | 25.1 | 2 763 (564, 881, 1 318) | 2.08% |
| $V_{\mathrm{VB}}$ | $10^{-2}$ | $10^{-2}$ | 58 | 25.4 | 3 336 (564, 348, 2 424) | 2.51% |
| $V_{\mathrm{WB}}$ | $10^{-2}$ | $10^{-2}$ | 50 | 26.4 | 5 189 (564, 4 156, 469) | 3.91% |
| Slab width $3h$ | | | | | | |
| $V_{\mathrm{AGDSW-S}}$ | $10^{-2}$ | $10^{-2}$ | 60 | 25.4 | 2 764 (564, 881, 1 319) | 2.08% |

TABLE 3

*Results for the coefficient function in Figure 8: iteration counts, condition number, and resulting coarse space dimension for different coarse spaces. Number of subdomains: 125; number of nodes: 132 651; $\delta = 1h$; maximum coefficient $A_{\max} = 10^6$; relative stopping criterion $\|r^{(k)}\|_2/\|r^{(0)}\|_2 < 10^{-8}$. Structured tetrahedral mesh; unstructured domain decomposition (METIS).*

requires 1 060 iterations to converge, while all adaptive coarse spaces converge in 60 iterations or less. In this particular example, the adaptive variants of GDSW lead to an increase of 39.1% in the coarse space dimension with respect to GDSW, whereas $V_{\mathrm{VB}}$ has a 67.9% and $V_{\mathrm{WB}}$ a 161.1% larger coarse space. Reducing the slab width of $V_{\mathrm{AGDSW-S}}$ to only $3h$ is sufficient to obtain almost identical results.

As a second example, we consider the coefficient function in Figure 9 with several layers of varying coefficients. We note that most of the domain is surrounded by a homogeneous Neumann boundary condition and the Dirichlet boundary does not touch a high coefficient layer; see Figure 9 (center). Despite a condition number of $3.8{\cdot}10^6$, the classical GDSW method requires only 125 iterations to converge, due to the relatively low number of coefficient jumps. For adaptive GDSW, we observe an increase in the coarse space dimension of only 13.7% compared to classical GDSW, while the dimension of $V_{\mathrm{VB}}$ is 59.3% larger and the wirebasket coarse space's dimension is more than twice as large as that of classical GDSW; cf. Table 4.

As a final realistic example, we consider a foam-like structure of high coefficients embedded in a cube; cf. Figure 10. We note that the foam structure consists of several disconnected smaller foam structures. The numerical results in Table 5 show that $V_{\mathrm{AGDSW}}$ converges within 61 iterations for a tolerance of 0.01, while increasing the coarse space dimension by only 22.5% compared to $V_{\mathrm{GDSW}}$. Using

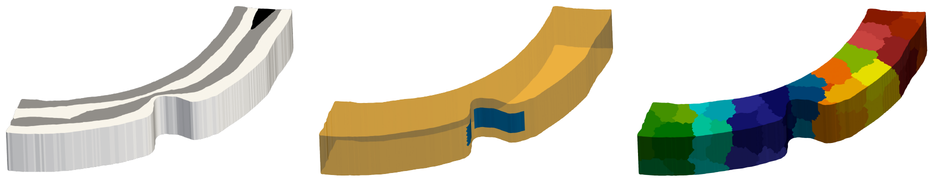

FIG. 9. ***(left)*** *Discontinuous coefficient function $A$ with coefficient layers of $A = 10^6$ in light gray and an inclusion at the top right with $A = 10^9$ in dark grey. The remainder of the coefficient in white is set to $A_{\min} = 1.0$.* ***(center)*** *Boundary partition for Dirichlet (blue) and Neumann (orange) boundary.* ***(right)*** *Domain decomposition of 50 subdomains. Number of nodes: 56 053; average number of nodes per subdomain: 1313.0; $\delta = 1h$. Unstructured tetrahedral mesh; unstructured domain decomposition (METIS).*

| | Coefficient function $A$ from Figure 9 | | | | | |
|---|---|---|---|---|---|---|
| $V_0$ | $tol_{\mathcal{E}}$ | $tol_{\mathcal{F}}$ | it. | $\kappa$ | $\dim V_0$ $(\mathcal{V},\mathcal{E},\mathcal{F})$ | $\dim V_0/\text{dof}$ |
| $V_{\text{GDSW}}$ | – | – | 125 | 3 770 557.2 | 445 (105, 168, 172) | 0.79% |
| $V_{\text{AGDSW}}$ | $10^{-2}$ | $10^{-2}$ | 50 | 20.1 | 506 (105, 186, 215) | 0.90% |
| $V_{\text{AGDSW-S}}$ | $10^{-2}$ | $10^{-2}$ | 50 | 20.1 | 506 (105, 186, 215) | 0.90% |
| $V_{\text{AGDSW-M}}$ | $10^{-3}$ | $10^{-3}$ | 50 | 20.1 | 506 (105, 186, 215) | 0.90% |
| $V_{\text{VB}}$ | $10^{-3}$ | $10^{-3}$ | 49 | 18.8 | 709 (105, 41, 563) | 1.26% |
| $V_{\text{WB}}$ | $10^{-3}$ | $10^{-3}$ | 41 | 15.0 | 964 (105, 854, 5) | 1.72% |
| Slab width $3h$ | | | | | | |
| $V_{\text{AGDSW-S}}$ | $10^{-2}$ | $10^{-2}$ | 50 | 20.1 | 506 (105, 186, 215) | 0.90% |

TABLE 4

*Results for the coefficient function in Figure 9: iteration counts, condition number, and resulting coarse space dimension for different coarse spaces. Number of subdomains: 50; number of nodes: 56 053; average number of nodes per subdomain: 1 313.0; $\delta = 1h$; maximum coefficient $A_{\max} = 10^9$; relative stopping criterion $\|r^{(k)}\|_2/\|r^{(0)}\|_2 < 10^{-8}$. Unstructured tetrahedral mesh; unstructured domain decomposition (METIS).*

a slab width of $3h$ and $V_{\text{AGDSW-S}}$ (and a tolerance of 0.01) results in an increase of the coarse space dimension with respect to GDSW by 23.6% and convergence is achieved within 60 iterations. In contrast, the coarse space $V_{\text{VB}}$ leads to an increase in the coarse space dimension of 104.1% while requiring 58 iterations to converge (tolerance: $10^{-5}$).

Finally, we present averaged results for 100 randomly generated coefficient functions with an average of 11.1% elements with high coefficients $A_{\max} = 10^6$ (the remainder is set to $A_{\max} = 1$). The results in Table 6 show that, also for random coefficient functions, the adaptive GDSW variants perform well. The largest coarse space dimension 13 665 of an adaptive GDSW variant is attained by restricting $V_{\text{AGDSW-S}}$ to a slab of width $3h$ ($tol_{\mathcal{E}} = tol_{\mathcal{F}} = 0.1$). This amounts to an increase of 36.2% compared to $V_{\text{GDSW}}$. Simultaneously, the largest number of iterations for this setting is 80, whereas classical GDSW did not converge within 2 000 iterations.

**10. Conclusion.** We have presented a new adaptive coarse space for the overlapping Schwarz method and proved a condition number bound. This bound depends on user prescribed tolerances but is independent of the mesh parameters $h$, $H$, and of heterogeneities in the coefficient function $A$.

At its core AGDSW uses generalized eigenvalue problems on edges and faces which are thus of moderate size compared to some competing approaches. AGDSW always contains the GDSW coarse space and only requires local nonoverlapping stiffness matrices to set up the eigenvalue problems; all other information can obtained algebraically. Several variants have been presented among which the one in subsection 7.2 facilitates the implementation and reduces the computational complexity by increasing sparsity.

The results in section 9 support the theory and show that using the discrete

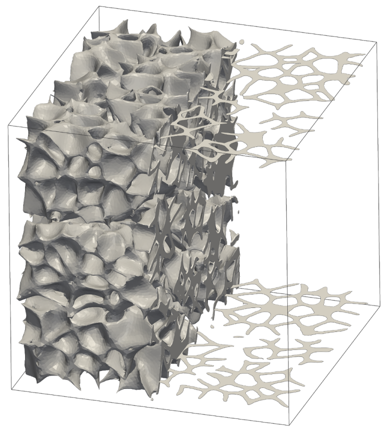

FIG. 10. *Partial visualization of an unstructured tetrahedral mesh consisting of several disconnected components of foam-like structures. In the corresponding mesh of a cube, the foam corresponds to a high coefficient of $A_{\max} = 10^6$ and is to $A_{\min} = 1.0$ elsewhere. The high coefficient does not touch the domain boundary. Number of subdomains: 100; number of nodes:* 588 958*; average number of nodes per subdomain:* 6 656.4*;* $\delta = 1h$*. Unstructured tetrahedral mesh; unstructured domain decomposition (METIS).*

| | Coefficient function $A$ from Figure 10 | | | | | |
|---|---|---|---|---|---|---|
| $V_0$ | $tol_{\mathcal{E}}$ | $tol_{\mathcal{F}}$ | it. | $\kappa$ | $\dim V_0$ $(\mathcal{V},\mathcal{E},\mathcal{F})$ | $\dim V_0/\mathrm{dof}$ |
| $V_{\mathrm{GDSW}}$ | – | – | 565 | 1 337 890.8 | 1 601 (404, 688, 509) | 0.27% |
| $V_{\mathrm{AGDSW}}$ | $10^{-2}$ | $10^{-2}$ | 61 | 30.7 | 1 962 (404, 741, 817) | 0.33% |
| $V_{\mathrm{AGDSW}}$ | $10^{-1}$ | $10^{-1}$ | 54 | 22.5 | 2 055 (404, 741, 910) | 0.35% |
| $V_{\mathrm{AGDSW-S}}$ | $10^{-2}$ | $10^{-2}$ | 61 | 30.7 | 1 963 (404, 742, 817) | 0.33% |
| $V_{\mathrm{AGDSW-S}}$ | $10^{-1}$ | $10^{-1}$ | 54 | 22.7 | 2 060 (404, 742, 914) | 0.35% |
| $V_{\mathrm{AGDSW-M}}$ | $10^{-3}$ | $10^{-3}$ | 61 | 30.7 | 1 962 (404, 741, 817) | 0.33% |
| $V_{\mathrm{AGDSW-M}}$ | $10^{-2}$ | $10^{-2}$ | 60 | 30.1 | 1 966 (404, 741, 821) | 0.33% |
| $V_{\mathrm{VB}}$ | $10^{-6}$ | $10^{-6}$ | 551 | 35 709.5 | 2 740 (404, 453, 1 883) | 0.47% |
| $V_{\mathrm{VB}}$ | $10^{-5}$ | $10^{-5}$ | 58 | 27.0 | 3 268 (404, 453, 2 411) | 0.55% |
| $V_{\mathrm{WB}}$ | $10^{-6}$ | $10^{-6}$ | 317 | 11 644.0 | 5 941 (404, 5 501, 36) | 1.01% |
| $V_{\mathrm{WB}}$ | $10^{-5}$ | $10^{-5}$ | 46 | 19.1 | 6 195 (404, 5 501, 290) | 1.05% |
| Slab width $3h$ | | | | | | |
| $V_{\mathrm{AGDSW-S}}$ | $10^{-2}$ | $10^{-2}$ | 60 | 29.7 | 1 979 (404, 744, 831) | 0.34% |
| $V_{\mathrm{AGDSW-S}}$ | $10^{-1}$ | $10^{-1}$ | 48 | 17.9 | 2 241 (404, 748, 1 089) | 0.38% |

TABLE 5

*Results for the coefficient function in Figure 10: iteration counts, condition number, and resulting coarse space dimension for different coarse spaces. Number of subdomains: 100; number of nodes:* 588 958*; average number of nodes per subdomain:* 6 656.4*;* $\delta = 1h$*; maximum coefficient* $A_{\max} = 10^6$*; relative stopping criterion* $||r^{(k)}||_2/||r^{(0)}||_2 < 10^{-8}$*. Unstructured tetrahedral mesh; unstructured domain decomposition (METIS).*

harmonic extension inside the eigenvalue problem (5) can help to reduce the dimension of the coarse space by detecting connected components of high coefficients. Furthermore, we have demonstrated the robustness of AGDSW for various realistic coefficient distributions.

## REFERENCES

[1] J. Aarnes and T. Y. Hou, *Multiscale domain decomposition methods for elliptic problems with high aspect ratios*, Acta Math. Appl. Sin. Engl. Ser., 18 (2002), pp. 63–76.

[2] P. Bjørstad, J. Koster, and P. Krzyzanowski, *Domain decomposition solvers for large scale industrial finite element problems*, in Applied Parallel Computing. New Paradigms for HPC in Industry and Academia, vol. 1947 of LNCS, Springer, Berlin, 2001, pp. 373–383.

[3] M. Buck, *Overlapping Domain Decomposition Preconditioners for Multi-Phase Elastic*

| | Random coefficient function $A$ | | | | | |
|---|---|---|---|---|---|---|
| $V_0$ | $tol_{\mathcal{E}}$ | $tol_{\mathcal{F}}$ | it. | $\kappa$ | $\dim V_0$ | $\dim V_0/\mathrm{dof}$ |
| $V_{\mathrm{GDSW}}$ | – | – | >2 000 ( – ) | $2.7\cdot10^5$ ($3.7\cdot10^5$) | 10 031.0 (10 031) | 2.2% (2.2%) |
| $V_{\mathrm{AGDSW}}$ | $10^{-1}$ | $10^{-1}$ | 79.4 ( 88) | 52.3 ( 74.6) | 13 244.3 (13 397) | 2.9% (3.0%) |
| $V_{\mathrm{AGDSW}}$ | $10^{-2}$ | $10^{-2}$ | 134.6 (158) | 166.9 ( 270.4) | 12 749.8 (12 963) | 2.8% (2.9%) |
| $V_{\mathrm{AGDSW-S}}$ | $10^{-1}$ | $10^{-1}$ | 74.3 ( 81) | 45.6 ( 68.8) | 13 438.0 (13 585) | 3.0% (3.0%) |
| $V_{\mathrm{AGDSW-S}}$ | $10^{-2}$ | $10^{-2}$ | 133.3 (157) | 164.5 ( 270.4) | 12 838.9 (13 043) | 2.8% (2.9%) |
| $V_{\mathrm{AGDSW-M}}$ | $10^{-2}$ | $10^{-2}$ | 113.1 (131) | 114.7 ( 169.5) | 12 825.2 (13 007) | 2.8% (2.9%) |
| $V_{\mathrm{AGDSW-M}}$ | $10^{-3}$ | $10^{-3}$ | 140.6 (165) | 187.5 ( 311.2) | 12 674.0 (12 879) | 2.8% (2.9%) |
| $V_{\mathrm{VB}}$ | $10^{-3}$ | $10^{-3}$ | 74.5 ( 87) | 54.6 ( 132.8) | 21 576.2 (22 147) | 4.8% (4.9%) |
| $V_{\mathrm{VB}}$ | $10^{-5}$ | $10^{-5}$ | 74.8 ( 87) | 55.6 ( 132.8) | 21 554.4 (22 144) | 4.8% (4.9%) |
| $V_{\mathrm{WB}}$ | $10^{-3}$ | $10^{-3}$ | 60.2 ( 72) | 36.0 ( 82.8) | 27 659.4 (27 884) | 6.1% (6.2%) |
| $V_{\mathrm{WB}}$ | $10^{-5}$ | $10^{-5}$ | 61.2 ( 72) | 39.5 ( 100.2) | 27 645.8 (27 880) | 6.1% (6.2%) |
| Slab width $3h$ | | | | | | |
| $V_{\mathrm{AGDSW-S}}$ | $10^{-1}$ | $10^{-1}$ | 71.7 ( 80) | 42.2 ( 62.2) | 13 526.3 (13 665) | 3.0% (3.0%) |
| $V_{\mathrm{AGDSW-S}}$ | $10^{-2}$ | $10^{-2}$ | 122.6 (137) | 137.4 ( 270.4) | 12 924.5 (13 109) | 2.9% (2.9%) |

TABLE 6

*Averaged results for 100 random coefficient functions (average high coefficient density:* 11.08%*): tolerance for the selection of the eigenfunctions, iteration counts, condition number, and resulting coarse space dimension for different coarse spaces; maximum in brackets. Number of subdomains: 512; number of nodes: 452 522; average number of nodes per subdomain: 1 174.4;* $\delta = 1h$*; maximum coefficient* $A_{\max} = 10^6$*; relative stopping criterion* $||r^{(k)}||_2/||r^{(0)}||_2 < 10^{-8}$*. Unstructured tetrahedral mesh; unstructured domain decomposition (METIS).* $V_{\mathrm{GDSW}}$ *never converged within 2 000 iterations.*

*Composites*, PhD thesis, Technische Universität Kaiserslautern, 2013.

[4] M. Buck, O. Iliev, and H. Andrä, *Multiscale finite elements for linear elasticity: Oscillatory boundary conditions*, in Domain Decomposition Methods in Science and Engineering XXI, J. Erhal, M. J. Gander, L. Halpern, G. Pichot, T. Sassi, and O. Widlund, eds., vol. 98 of LNCSE, Springer, 2014, pp. 237–245.

[5] C. Dohrmann and O. B. Widlund, *An alternative coarse space for irregular subdomains and an overlapping Schwarz algorithm for scalar elliptic problems in the plane*, SIAM Journal on Numerical Analysis, 50 (2012), pp. 2522–2537.

[6] C. R. Dohrmann, A. Klawonn, and O. B. Widlund, *Domain decomposition for less regular subdomains: overlapping Schwarz in two dimensions*, SIAM J. Numer. Anal., 46 (2008), pp. 2153–2168.

[7] C. R. Dohrmann, A. Klawonn, and O. B. Widlund, *A family of energy minimizing coarse spaces for overlapping Schwarz preconditioners*, in Domain decomposition methods in science and engineering XVII, vol. 60 of Lect. Notes Comput. Sci. Eng., Springer, Berlin, 2008, pp. 247–254.

[8] C. R. Dohrmann and O. B. Widlund, *An overlapping Schwarz algorithm for almost incompressible elasticity*, SIAM Journal on Numerical Analysis, 47 (2009), pp. 2897–2923.

[9] C. R. Dohrmann and O. B. Widlund, *Hybrid domain decomposition algorithms for compressible and almost incompressible elasticity*, Internat. J. Numer. Meth. Engng., 82 (2010), pp. 157–183.

[10] C. R. Dohrmann and O. B. Widlund, *A BDDC algorithm with deluxe scaling for three-dimensional H(curl) problems*, Communications on Pure and Applied Mathematics, 69 (2016), pp. 745–770.

[11] C. R. Dohrmann and O. B. Widlund, *On the design of small coarse spaces for domain decomposition algorithms*, SIAM J. Sci. Comput., 39 (2017), pp. A1466–A1488.

[12] V. Dolean, F. Nataf, R. Scheichl, and N. Spillane, *Analysis of a two-level Schwarz method with coarse spaces based on local Dirichlet-to-Neumann maps*, Comput. Methods Appl. Math., 12 (2012), pp. 391–414.

[13] M. Dryja and O. B. Widlund, *Domain decomposition algorithms with small overlap*, SIAM J. Sci.Comput., 15 (1994), pp. 604–620.

[14] Y. Efendiev, J. Galvis, R. Lazarov, and J. Willems, *Robust domain decomposition preconditioners for abstract symmetric positive definite bilinear forms*, ESAIM: Mathematical Modelling and Numerical Analysis, 46 (2012), pp. 1175–1199.

[15] Y. Efendiev and T. Y. Hou, *Multiscale Finite Element Methods: Theory and Applications*, Surveys and Tutorials in the Applied Mathematical Sciences, Springer New York, 2009.

[16] E. Eikeland, L. Marcinkowski, and T. Rahman, *Overlapping Schwarz methods with adaptive coarse spaces for multiscale problems in 3D*, tech. report, arxiv.org, 2016, arXiv:1611.00968.

[17] J. Galvis and Y. Efendiev, *Domain decomposition preconditioners for multiscale flows in*

*high contrast media: reduced dimension coarse spaces*, Multiscale Modeling & Simulation, 8 (2010), pp. 1621–1644.

[18] M. J. Gander and A. Loneland, *SHEM: An optimal coarse space for RAS and its multiscale approximation*, in Domain Decomposition Methods in Science and Engineering XXIII, C.-O. Lee, X.-C. Cai, D. E. Keyes, H. H. Kim, A. Klawonn, E.-J. Park, and O. B. Widlund, eds., vol. 116 of LNCSE, Springer, 2017, pp. 313–321.

[19] M. J. Gander, A. Loneland, and T. Rahman, *Analysis of a new harmonically enriched multiscale coarse space for domain decomposition methods*, tech. report, arxiv.org, 2015.

[20] I. Graham, P. Lechner, and R. Scheichl, *Domain decomposition for multiscale PDEs*, Numerische Mathematik, 106 (2007), pp. 589–626.

[21] A. Heinlein, *Parallel Overlapping Schwarz Preconditioners and Multiscale Discretizations with Applications to Fluid-Structure Interaction and Highly Heterogeneous Problems*, PhD thesis, University of Cologne, 2016.

[22] A. Heinlein, C. Hochmuth, and A. Klawonn, *Monolithic overlapping Schwarz domain decomposition methods with GDSW coarse spaces for saddle point problems*, Tech. Report CDS-TR 2018-1, preprint at http://kups.ub.uni-koeln.de/id/eprint/8355, University of Cologne, Center for Data and Simulation Science, 2018. Submitted 07/2018 to SIAM J. Sci. Comput.

[23] A. Heinlein, A. Klawonn, J. Knepper, and O. Rheinbach, *An adaptive GDSW coarse space for two-level overlapping Schwarz methods in two dimensions*, in Domain Decomposition Methods in Science and Engineering XXIV, vol. 125 of LNCSE, Springer, 2018. Accepted 02/2018 for publication.

[24] A. Heinlein, A. Klawonn, J. Knepper, and O. Rheinbach, *Multiscale coarse spaces for overlapping Schwarz methods based on the ACMS space in 2D*, Electron. Trans. Numer. Anal., 48 (2018), pp. 156–182.

[25] A. Heinlein, A. Klawonn, S. Rajamanickam, and O. Rheinbach, *FROSch – a parallel implementation of the GDSW domain decomposition preconditioner in Trilinos.* In Preparation.

[26] A. Heinlein, A. Klawonn, and O. Rheinbach, *A parallel implementation of a two-level overlapping Schwarz method with energy-minimizing coarse space based on Trilinos*, SIAM J. Sci. Comput., 38 (2016), pp. C713–C747.

[27] A. Heinlein, A. Klawonn, and O. Rheinbach, *Parallel two-level overlapping Schwarz methods in fluid-structure interaction*, in Numerical Mathematics and Advanced Applications ENUMATH 2015, B. Karasözen, M. Manguoğlu, M. Tezer-Sezgin, S. Göktepe, and Ö. Uğur, eds., vol. 112 of LNCSE, Springer, 2016, pp. 521–530.

[28] A. Heinlein, A. Klawonn, and O. Rheinbach, *Parallel overlapping Schwarz with an energy-minimizing coarse space*, in Domain Decomposition Methods in Science and Engineering XXIII, C.-O. Lee, X.-C. Cai, D. E. Keyes, H. H. Kim, A. Klawonn, E.-J. Park, and O. B. Widlund, eds., vol. 116 of LNCSE, Springer, 2017, pp. 353–360.

[29] A. Heinlein, A. Klawonn, O. Rheinbach, and F. Röver, *A three-level extension of the GDSW overlapping Schwarz preconditioner in 2D*, Tech. Report Preprint 2018-04 at http://tu-freiberg.de/fakult1/forschung/preprints, 2018. Submitted 03/2018 to LNCSE.

[30] A. Heinlein, A. Klawonn, O. Rheinbach, and O. Widlund, *Improving the parallel performance of overlapping Schwarz methods by using a smaller energy minimizing coarse space*, in Domain Decomposition Methods in Science and Engineering XXIV, vol. 125 of LNCSE, Springer, 2018. Accepted 02/2018 for publication.

[31] M. A. Heroux, R. A. Bartlett, V. E. Howle, R. J. Hoekstra, J. J. Hu, T. G. Kolda, R. B. Lehoucq, K. R. Long, R. P. Pawlowski, E. T. Phipps, A. G. Salinger, H. K. Thornquist, R. S. Tuminaro, J. M. Willenbring, A. Williams, and K. S. Stanley, *An overview of the Trilinos project*, ACM Trans. Math. Softw., 31 (2005), pp. 397–423.

[32] U. L. Hetmaniuk and R. B. Lehoucq, *A special finite element method based on component mode synthesis*, M2AN Math. Model. Numer. Anal., 44 (2010), pp. 401–420.

[33] T. Y. Hou and X.-H. Wu, *A multiscale finite element method for elliptic problems in composite materials and porous media*, J. Comput. Phys., 134 (1997), pp. 169 – 189.

[34] G. Karypis and V. Kumar, *A fast and high quality multilevel scheme for partitioning irregular graphs*, SIAM J. Sci. Comput, 20 (1998), pp. 359–392.

[35] H. H. Kim, E. Chung, and J. Wang, *BDDC and FETI-DP preconditioners with adaptive coarse spaces for three-dimensional elliptic problems with oscillatory and high contrast coefficients*, J. Comput. Phys., 349 (2017), pp. 191–214.

[36] A. Klawonn, M. Kühn, and O. Rheinbach, *Adaptive coarse spaces for FETI-DP in three dimensions*, SIAM J. Sci. Comput., 38 (2016), pp. A2880–A2911.

[37] A. Klawonn, M. Kühn, and O. Rheinbach, *Adaptive FETI-DP and BDDC methods with a generalized transformation of basis for heterogeneous problems*, Electron. Trans. Numer. Anal., 49 (2018), pp. 1–27.

[38] A. Klawonn, P. Radtke, and O. Rheinbach, *A comparison of adaptive coarse spaces for iterative substructuring in two dimensions*, Electron. Trans. Numer. Anal., 45 (2016), pp. 75–106.

[39] A. Klawonn and O. Rheinbach, *A parallel implementation of dual-primal FETI methods for three dimensional linear elasticity using a transformation of basis*, SIAM J. Sci. Comput., 28 (2006), pp. 1886–1906.

[40] A. Klawonn and O. Rheinbach, *Robust FETI-DP methods for heterogeneous three dimensional elasticity problems*, Comput. Methods Appl. Mech. Engrg., 196 (2007), pp. 1400–1414.

[41] A. Klawonn and O. Widlund, *Dual-primal FETI methods for linear elasticity*, Comm. Pure Appl. Math., 59 (2006), pp. 1523–1572.

[42] A. V. Knyazev, *Toward the optimal preconditioned eigensolver: locally optimal block preconditioned conjugate gradient method*, SIAM J. Sci. Comput., 23 (2001), pp. 517–541.

[43] J. Mandel and B. Sousedík, *Adaptive selection of face coarse degrees of freedom in the BDDC and the FETI-DP iterative substructuring methods*, Comput. Methods Appl. Mech. Engrg., 196 (2007), pp. 1389–1399.

[44] J. Mandel, B. Sousedík, and J. Šístek, *Adaptive BDDC in three dimensions*, Mathematics and Computers in Simulation, 82 (2012), pp. 1812–1831.

[45] L. Marcinkowski and T. Rahman, *Additive average Schwarz with adaptive coarse spaces: scalable algorithms for multiscale problems*, Electron. Trans. Numer. Anal., 49 (2018), pp. 28–40.

[46] C. Pechstein and C. Dohrmann, *Modern domain decomposition solvers - BDDC, deluxe scaling, and an algebraic approach.* Slides to a talk at NuMa Seminar, JKU Linz, December 10th, 2013, http://people.ricam.oeaw.ac.at/c.pechstein/pechstein-bddc2013.pdf.

[47] C. Pechstein and C. R. Dohrmann, *A unified framework for adaptive BDDC*, Electron. Trans. Numer. Anal., 46 (2017), pp. 273–336.

[48] S. Rajamanickam, E. G. Boman, and M. A. Heroux, *ShyLU: A hybrid-hybrid solver for multicore platforms*, in 2012 IEEE 26th International Parallel and Distributed Processing Symposium, May 2012, pp. 631–643.

[49] Y. Saad, *Iterative Methods for Sparse Linear Systems*, SIAM, second ed., 2003.

[50] B. Smith, P. Bjørstad, and W. Gropp, *Domain Decomposition: Parallel Multilevel Methods for Elliptic Partial Differential Equations*, Cambridge University Press, 1996.

[51] N. Spillane, V. Dolean, P. Hauret, F. Nataf, C. Pechstein, and R. Scheichl, *Abstract robust coarse spaces for systems of PDEs via generalized eigenproblems in the overlaps*, Numerische Mathematik, 126 (2014), pp. 741–770.

[52] N. Spillane and D. Rixen, *Automatic spectral coarse spaces for robust finite element tearing and interconnecting and balanced domain decomposition algorithms*, International Journal for Numerical Methods in Engineering, 95 (2013), pp. 953–990.

[53] A. Toselli and O. Widlund, *Domain decomposition methods—algorithms and theory*, vol. 34 of Springer Series in Computational Mathematics, Springer-Verlag, Berlin, 2005.

[54] R. Verfürth, *A posteriori error estimation techniques for finite element methods*, Numerical Mathematics and Scientific Computation, Oxford University Press, Oxford, 2013.